Autumn and Winter storms over UK and Ireland are becoming wetter due to climate change

Authors

Sarah F. Kew, *Royal Netherlands Meteorological Institute (KNMI), De Bilt, The Netherlands*
Mark McCarthy, *Met Office, Exeter, UK*
Ciara Ryan, *Met Éireann, Dublin, Ireland*
Jennifer S.R. Pirret, *Met Office, Exeter, UK.*
Ellie Murtagh, *British Red Cross, London, UK (based in Edinburgh, UK)*
Maja Vahlberg, *Red Cross Red Crescent Climate Centre, the Hague, Netherlands (based in Ubmeje/Umeå, Sweden)*
Adwoa Amankona, *Red Cross Red Crescent Climate Centre, the Hague, Netherlands (based in London, UK)*
James O. Pope, *Met Office, Exeter, UK.*
Fraser Lott, *Met Office, Exeter, UK*
Oliver Claydon, *Met Office, Exeter, UK.*
Barry Coonan, *Met Éireann, Dublin, Ireland*
Izidine Pinto, *Royal Netherlands Meteorological Institute (KNMI), De Bilt, The Netherlands*
Clair Barnes*, Grantham Institute, Imperial College London, UK*
Sjoukje Philip, *Royal Netherlands Meteorological Institute (KNMI), De Bilt, The Netherlands*

Review authors

Fredi Otto, *Grantham Institute, Imperial College London, UK*
Emily Wallace, *Met Office, Exeter, UK.*
Leo Bryant, *British Red Cross, London, UK*
Ellen Tranter, *British Red Cross, London, UK*
Roop Singh, *Red Cross Red Crescent Climate Centre, the Hague, Netherlands*
Ana Mijic, *Faculty of Engineering, Department of Civil and Environmental Engineering, Imperial College London, UK*

Main findings

- The 2023/24 storm season, studied here by stormy day wind severity, associated rainfall, and accumulated seasonal rainfall in October-March, has brought deaths, flooding, transport disruptions and power outages, among other impacts, to the UK and Ireland.

- Successive floods have compounded impacts on the agriculture and housing sectors, leading to cascading impacts on socioeconomic and psychosocial health, and eroding people's coping capacity, particularly low-income groups. Combined with the cost-of-living crisis, the successive flood events are another layer of disruption at a time when people's financial resilience is already being tested.
- The storm severity index (SSI) was used to define stormy days to study. The SSI considers both the strength of the wind and the area affected. In this analysis we looked at rainfall and wind speed on stormy days identified by the SSI.
- In today's climate with 1.2C of warming, stormy days with winds as intense as in the 2023/24 season occur about every 4 years. The associated precipitation is expected to occur about once every 5 years. The seasonal precipitation of the October-March period was more extreme, expected to occur about once every 20 years.
- Analyses of observations are used to determine whether a trend can be observed in these measures. To determine the role of climate change in these observed changes, we combine observations with climate models.
- The average precipitation on stormy days are observed to have become approximately 35% more intense, compared to a 1.2C cooler pre-industrial climate. Models agree on the direction of change, combining observations and models indicate that average precipitation on stormy days increased by about 20% due to human induced climate change, or equivalently the 2023/24 level has become about a factor of 10 more likely.
- The observed precipitation across Oct-Mar has a strong trend, with a magnitude increase of about 25%. Climate models utilised in this study broadly agree on the direction of the change, and the combination of observation and model results indicates an increase in magnitude of 6% to 25%, or equivalently the 2023/24 level has become at least a factor of 4 more likely.
- Models indicate that the trends in average precipitation on stormy days and seasonal precipitation continue into the future, in a climate that is 0.8C warmer than now. Average precipitation on stormy days becomes about another factor of 1.6 times more likely, or 4% more intense, and seasonal precipitation becomes about a factor of 1.5 more likely or 2% more intense.
- Looking at average SSI on storm days, while some studies using other methods suggest an increase in storminess in a future climate, our analysis has shown a decreasing trend. Our results show that average SSI indices as observed this year became about a factor of 2 less likely. The synthesis of the models also shows a negative trend and, when combined with observations, the results indicate that a stormy season as observed this year is nowadays a factor of about 1.4 less likely due to human induced climate change.
- This highlights the need for ongoing research into how climate change may influence the severity and frequency of windstorms in northern Europe.
- NAO is a key driver of 'storminess' and has been accounted for in this analysis. However, the Oct-Mar 2023/24 averaged NAO was almost neutral.
- Comprehensive flood risk management is required in the UK and Ireland that encompasses legislative frameworks, strategic planning, and substantial funding. Major UK cities are starting to integrate nature-based solutions into their designs. In Ireland, flood relief projects have been integrating nature-based solutions alongside

traditional engineering solutions for over 20 years. Both the UK Met Office and Met Éireann are continuously improving their impact-based weather forecasting mechanisms to facilitate the translation of warning into action, in partnership with other government bodies to ensure their people's safety.

1 Introduction

During the autumn and winter of 2023/24, western Europe experienced a series of damaging storms. Storms of this nature are common over the European region during Autumn and Winter, being low atmospheric pressure systems that typically develop over the North Atlantic Ocean, then move eastwards over Europe bringing strong winds accompanied in cases by heavy rainfall. This eastward movement is driven by the polar jet stream, a band of strong westerly winds high up in the atmosphere. The 2023/24 storm season is the ninth season since the founding of the Western Europe storm naming group. The initiative began in 2015, when the Met Office and Met Éireann, Ireland's national meteorological service, officially started naming storms to aid communication of severe weather events. In 2019, the Royal Netherlands Meteorological Institute (KNMI) joined the Western Group. Together, the three meteorological organisations collaborate to identify and name storms that have the potential to cause medium or high impacts.

The 2023/24 storm season was notable for the number of storms that met the threshold required for naming in western Europe (11 to date named by this group, 14 impacting the domain under study). This study was triggered by four such storms: Babet, Ciarán, Henk (named by the Met Office in the UK) and Ingunn (named by Norwegian Meteorological Institute). Each of these storms brought high winds and heavy rainfall, but it varied between storms which hazard dominated and which region was most affected. Furthermore, their impacts, especially for rainfall, were exacerbated by rainfall from a series of synoptic systems affecting a similar area in quick succession, leaving the ground saturated and unable to absorb any new rainfall, increasing surface runoff and flood risk.

There is considerable inter-annual variability of winter storms over western Europe (Feser et al., 2015), with different numbers of named storms each year ranging from 2 [4] to 11 [14] (to date, where the number of storms named by the Western Europe group is quoted first, with the total including any storms adopted by other groups given in square brackets). The current season which runs from 1st September 2023 to 31st August 2024 has been marked by a series of storms, with widespread impacts across the region. To date, in the 2023/24 season there have been eleven named storms by the Western Europe naming group. The latest storm at time of publication, Storm Kathleen, was named by Met Éireann on 6th April 2024, just the second occurrence of reaching the letter "K" since the storm naming initiative began in 2015. Starting with Storm Debi (the fourth named storm of the season), the naming of this season's storms, up to and including Storm Jocelyn (the tenth named storm), have occurred earlier in the season than in any previous season. That is, Storm Debi is the earliest that the Western Group has reached the letter 'D' on the storm naming list, Storm Elin is the earliest that the letter 'E' has been reached and so on. In contrast to the busy 2023/24 season, the previous storm season (2022/23) saw only two named storms by the Western Group across the year, with these storms coming late in the season - both Storm Antoni and Storm Betty impacted Ireland and the UK in August 2023 (although Ireland was impacted by a total of 4 storms that season, with Otto and Noa adding to Antoni and Betty) .

The storminess of the 2023/24 season so far has been primarily dictated by the position and strength of the jet stream, which is driven by temperature differences between the equator and the poles and tends to be strongest in winter when the temperature difference is greatest. The position of the jet stream influences how many low-pressure systems are directed towards Ireland and the UK. The strength of the jet stream, and how each individual low-pressure system interacts with it, determines whether these low-pressure systems intensify enough to become Atlantic storms. During the 2023-24 season, the jet stream was stronger than normal, which likely contributed to how strong the storms became. In January 2024, the jet stream was intensified by a large contrast in temperature across North America caused by a pool of cold air over Canada and the United States sinking south. This influenced the development of both Storms Isha and Jocelyn, the ninth and tenth named storms of the 2023/24 storm season, which arrived in quick succession in late January 2024.

The North Atlantic Oscillation is a mode of natural variability, commonly defined as the normalised pressure gradient between Iceland and the Azores, is also related to the degree of storminess and the position of the jet stream, with positive values meaning westerly winds dominate across the Atlantic and a stronger jet stream, which typically brings mild, wet and stormy conditions to western Europe (e.g. Hall et al., 2017). Variations in the jet stream are further influenced by interactions between many different components and drivers of the global weather system such as sea surface temperatures (e.g. Hall et al., 2017), the El Niño-Southern Oscillation (e.g. Manney et al., 2021), and the Stratospheric Polar Vortex (e.g. Kidston et al., 2015) in winter. The complex interplay between these systems means that northern European storminess exhibits considerably inter-annual and decadal variability, this means it is difficult to robustly detect trends (Kendon et al. 2023) and is also a major challenge in modelling potential future changes in storminess (Pirret et al. 2023).

Four of the named storms from the 2023/24 season exposed large populations to hazardous conditions and had significant socio-economic impacts that met the storm trigger criteria of the World Weather Attribution (WWA) group. These were the storms Babet, Ciarán, Henk, and Ingunn. We describe these four storms and their impacts below, with a summary of all named storms that impacted the UK and Ireland given in Table 1.

North Atlantic storm systems also bring rain, and associated impacts, to Ireland and the UK. From a rainfall point of view, October 2023 to March 2024 was the second wettest Oct-Mar period on record for the UK and the third wettest for Ireland (see Fig. 1 for the Oct-Mar precipitation anomalies). Given the apparent intensity of this year's storm season particularly from the standpoint of rainfall, we choose to study the wet season, focussing on storms and precipitation occurring between October and March. With the exception of Babet (Clarke et al., 2024), the triggered storms have not been studied individually by WWA.

Babet

Storm Babet was the second named storm of the 2023/24 storm season. Storm Babet was an extratropical cyclone that impacted Ireland and the UK on 18th-21st October. Extratropical storms are a common occurrence at this time of year in this region. Typically, however, Atlantic storm systems affecting Ireland and the UK in the autumn and winter months track west to east, driven by the jet stream, clearing eastwards quickly. This storm was on an unusual track from south to north, enabling it to pick up additional moisture as it crossed the Bay of Biscay. Due to a blocking area of high pressure across Scandinavia, Babet also stalled longer over the UK and Ireland than typical Atlantic

storms. Significant amounts of rainfall fell over the course of the storm which led to widespread and severe impacts across Ireland and the UK, particularly in the south of Ireland and eastern Scotland. Storm Babet also brought some powerful winds, gusting at over 50 knots (92.6 km/h) across northeast England and much of Scotland.

In the UK, two rare red weather warnings were issued for parts of eastern Scotland and particularly the county of Angus (Met Office, 2023), with amber or yellow warnings issued mainly over Scotland and northern England. The impacts included: seven people who died; hundreds of flooded homes and businesses with particularly severe effects in the town of Brechin (in Angus) where flood defences were overtopped; transport disruption including closure of trunk roads and mainline railways, and cancellation of ferries to the Scottish islands; and 30,000 homes losing power in northern Scotland. In the Netherlands, the synoptic low pressure brought high winds and large amounts of rain to the country. An exceptionally strong easterly wind caused extremely low water levels in the Frisian Islands region, leading to cancellation of ferry services to some of the islands. In Ireland, Storm Babet brought record rainfall amounts leading to significant flooding, with the town of Midleton, County Cork severely impacted. In Midleton alone, about 395 residential properties and 286 commercial properties flooded during Storm Babet. The intense 2-day rainfall fell on soils saturated by over 3 months of above average rainfall that started with the wettest July on record nationally. Peak river flows coincided with a low spring tide, meaning that the river was able to drain into the sea. Had the event occurred at high tide and/or with substantial storm surge, flooding could have been much more extensive.

Preceding Babet, in the summer of 2023, unprecedented temperatures were measured in the northern Atlantic (Met Éireann, 2023), projecting onto a positive phase of the Atlantic Multidecadal Variability (AMV). The exceptional warmth of the Atlantic may have played a role in the amplification of Babet and in the amount of precipitation that fell particularly over eastern Scotland (Thompson et al., 2024). See section 3.4 for further details on the connection with the AMV.

Ciarán

Storm Ciarán was named by the Met Office on 29th October 2023. The powerful storm swept in from the Atlantic over northern France, the Channel Islands and southern England, bringing with it strong winds and heavy rainfall. The storm underwent ‘explosive cyclogenesis’ as it approached the UK, deepening rapidly and gaining strength. Storm Ciarán set a new record for the lowest mean sea level pressure recorded in England, breaking the previous record from 1916. Winds across northern France and the Channel Islands were particularly severe, comparable in severity with those experienced in the south-east of England during the ‘Great Storm’ of 16 October 1987. Storm Ciarán also brought heavy rainfall, with flood risk exacerbated by saturated ground conditions and high river levels resulting from the wet weather experienced throughout October. In the UK, weather warning levels reached amber for wind in southern England, with yellow wind and rain warnings affecting southern England, Wales and Northern Ireland. These were the areas that experienced the greatest impacts, with disruption including closing the port of Dover, cancellation of trains and flights in southern England, school closures, 150,000 properties losing power including at three water treatment plants, which in turn left thousands without water supply. Jersey’s meteorological service issued a red warning, and the government declared a major incident advising only essential travel with the closure of major roads, shops, schools, and the airport (BBC, 2023a). Impacts included damage to properties and infrastructure (particularly roads) from falling trees, and power outages (BBC, 2023b; BBC, 2023c). In the Netherlands, 'code orange warnings' were given for very strong wind gusts in coastal regions with 'code yellow' warnings for wind in the rest of the country. Across western Europe, impacts

included at least 13 deaths linked to the heavy rain and flooding resulting from storm Ciarán (Met Office, 2023).

Henk

Storm Henk was named by the Met Office on the 2nd January 2024. The storm tracked rapidly eastwards, staying off the south coast of Ireland before reaching southern England and moving up from the south-west to north-east of the UK. Storm Henk brought damaging winds and heavy rain to southern regions of England and Wales (Met Office, 2024). Winds of 50 knots (92.6 km/h) gusted across inland areas, with a fastest wind gust of 70 knots (129.6 km/h) recorded at Exeter Airport. Heavy rainfall was observed across much of England and Wales with the highest totals seen in south west England, western and southern Wales and south central England, with between 50 and 100 mm of rain falling widely across these areas. For wind, a yellow warning covered much of southern Wales, southern England and the Midlands, with an amber warning embedded within it; for rain, a yellow warning covered Wales and a large part of the southern half of England. In the Netherlands, code orange warnings for very strong wind gusts were given in the northeast regions. The storm caused fallen trees and branches on roads, and minor damage to buildings. Public transport operated with an adjusted timetable.

Ingunn

Rapidly deepening storm Ingunn was named by the Norwegian Meteorological Institute (NMI) on 30 January 2024 (NMI, 2024). NMI issued red warnings for hurricane force winds and avalanches in Norway. Yellow warnings were issued by the Met Office for Scotland and parts of northern England and Northern Ireland for 31 January with forecasts of severe gales and wind gusts exceeding 100 mph (87 knots, 161.1 km/h) (Met Office, 2024) and tornado warnings (Daily Mail, 2024). Flights and ferry travel were disrupted (Yahoo News, 2024). Further impacts to the UK included cancellations and speed restrictions of ScotRail trains, closing of attractions such as castles and zoos, and closed schools and nurseries in the Western Isles and Highlands (Daily Mail, 2024). 155 mph (135 knots, 250.0 km/h) winds were recorded in the Faroe Islands, to the north of our study domain.

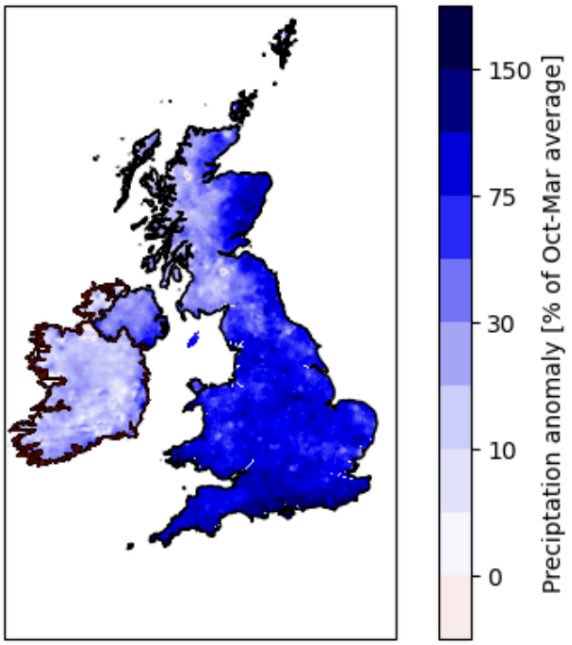

Figure 1. Precipitation anomaly [%] relative to the Oct-Mar average over the years 1991/1992 to 2020/2021. Source: Met Office HadUK-Grid and Met Éireann's gridded precipitation datasets.

1.1 Event definition

This study requires a method to identify storms which is systematic, representative of impactful extreme events, and readily derivable from observational data and climate models. Rather than identify individual storms through sea-level pressure minima or measures of circulation, which would be computationally demanding and require post-processing to relate the output to impacts, we use the established Storm Severity Index (SSI, see Section 2.3 for further details) as a measure of storminess over a region. The SSI is based on the cube of wind speed, which is commonly used for damage studies, as described in Leckebusch et al., (2008) and utilised in studies of wind events under a changing climate (e.g. Bloomfield et al., 2024). The SSI quantifies by how much the wind speed on a given day exceeds the 98th percentile of winter wind speeds, so highlights the 2% of days in the winter half-year which previous studies have assumed cause wind damage (Klawa and Ulbrich, 2003). This is done point-by-point, so summing over the area also indicates how much of the domain is affected by potentially damaging wind speeds.

To approximately capture the number of named storms per season, we use a baseline threshold of SSI – the 90th percentile of SSI calculated over the years 1979-2020 – to define a stormy day for the study region as a whole. The study region, a box (50N-61N, 11W-2E) chosen to encompass the main land masses of the United Kingdom and Ireland, is called the UKIre region in the remainder of this paper. Furthermore, we split the UKIre region at latitude 54N into two separate regions to test whether north and south subdomains show different results. A North-South division is motivated by possible latitudinal shifting of the jet stream and the jet stream's influence on storminess. These regions are called the North region and the South region.

We use three event definitions:

1. The average SSI on stormy days per Oct-Mar season
2. The average precipitation over land on stormy days per Oct-Mar season
3. The Oct-Mar total precipitation averaged over land in the study region

Note that while the SSI is calculated over the whole of the study region, the precipitation indices are only calculated over land. This is for a couple of reasons: the national precipitation gridded products, considered to be the best local records, are for land only; and the impacts of heavy precipitation are essentially land-based.

Table 1. *Named storms with notable impacts on the UK or Ireland. Names of WWA-triggered storms are emphasised in bold. Colour indicates the naming group: blue - the Western Europe storm naming group, green - Météo-France, red - Norwegian Meteorological Institute. The last column indicates whether the storm is captured by the SSI threshold used here, using the date ranges of impacts of the named storms given by the Met Office, and the date of maximum impact of storms named by Météo-France, and Norwegian Meteorological Institute, each expanded by 1 day each way.*

Name of storm	Date (impact UK/Ireland)	Notable impacts to UK/Ireland	Captured by SSI threshold
Agnes	27-28 Sep	In Ireland: widespread power outages and flooding, travel disruptions and significant structural damages. In UK: power outages and travel disruption for Cumbria and south-west Scotland.	Excluded, not in Oct-Mar.
Babet	18-21 Oct	In south-west Ireland: significant flooding leading to severe damage to properties and infrastructure. In UK: Widespread flooding affecting properties and transport, and resulting in seven fatalities	UK+Ire, north, south
Ciarán	1-2 Nov	In southern England: Transport disruption, school closures, power	UK+Ire, south

		outages, property damage. Power outage at three water works cutting off water supply for thousands. Channel Islands and north France: Worst impacted regions. Property damage. 1.2 million people without power. A Tornado in Jersey. In Ireland: some travel disruptions, flight and ferry delays.	
Debi	13 Nov	In Ireland: Flood damage to homes and businesses in the west of Ireland. Storm surge caused significant damage and partial collapse of the sea wall in Co. Galway. Fallen trees and wires caused travel disruptions.	-
Elin	9 Dec	In Ireland: Travel disruption, flight cancellations, fallen trees and power outages.	north
Fergus	10 Dec	In Ireland: fallen trees, power outages and some tidal flooding in Co. Galway.	-
Gerrit	27-28 Dec	In Ireland: power outages, flight and ferry delays, some fluvial and coastal flooding. In UK: Travel disruption due to landslips, flooding and trees blown over. Tornado caused damage in Manchester.	UK+Ire, north, south

Henk	2-3 Jan	In UK: Power outages and transport disruption. Almost 300 flood warnings in place across England plus others in Wales and Scotland. Some properties flooded for the fourth time in the winter.	UK+Ire, north, south
Isha	21-22 Jan	In Ireland: Three people died in road accidents during Storm Isha. Widespread travel disruption, flight cancellations, fallen trees, damage to infrastructures, power outages and water supply interruptions. In UK: Widespread fallen trees, damage to buildings and transport disruption. Hundreds of thousands of properties in Scotland, Northern Ireland, north-west England and Wales experienced loss of power. Operations at Sellafield Nuclear plant suspended.	UK+Ire, north, south
Jocelyn	23-24 Jan	In UK: This storm hampered the clean up operation from storm Isha. In Ireland: flight cancellations, fallen trees, further damages to already weakened infrastructure from Storm Isha, and further power outages as well as delays restoring power lost during storm Isha.	UK+Ire, north, south

Kathleen	6-7 Apr	In UK: Cancellations of some flights and ferries. In Ireland: flight and ferry cancellations, damage to infrastructure, travel disruptions, widespread power outages.	Excluded, not in Oct-Mar.
Elisa	9 Nov	In Ireland: travel disruptions	south
Geraldine	31 Dec	In Ireland: travel disruptions.	UK+Ire, north, south
Ingunn	31 Jan	In UK: travel disruptions and cancellations.	UK+Ire, north

2 Data and methods

2.1 Observational data

ERA5

The European Centre for Medium-Range Weather Forecasts's 5th generation reanalysis product, ERA5, is a gridded dataset that combines historical observations into global estimates using advanced modelling and data assimilation systems (Hersbach et al., 2020). We use 10-m wind and mean sea level pressure (MSLP) data from this product at a resolution of 0.25°×0.25°, from the years 1951 to present.

HadUK-Grid precipitation data set

The Met Office HadUK-Grid dataset (Hollis et al. 2019) provides a gridded 1km x 1km daily rainfall product for the period 1891-present. The underlying station data is the Met Office Integrates Data Archive System (MIDAS) Land and Marine Surface station database (Met Office, 2012). The data are interpolated onto a fixed grid on a British National Grid projection. Version 1.2.0.0 is utilised here for data up to and including calendar year 2022 (Met Office, 2023), with data for 2023 and 2024 based on provisional data (Met Office Hadley Centre observations datasets). The number of available daily rain gauge records in the digital archive drops significantly before 1960 so should be interpreted with caution when comparing trends in extreme precipitation before and after 1960 (Simpson and McCarthy, 2018). The current observing network for the UK includes over 2000 rain gauges.

Met Éireann gridded precipitation data set

Met Éireann's 1 km x 1 km gridded daily precipitation dataset for the period 1941-2024 was used to calculate aggregated precipitation values over Ireland including mean daily rainfall totals north and south of latitude 54N. The same daily precipitation grids were used to map storm events from October 2023 to March 2024 with a gridded 30-year climatology based on the period October 1991 - March 1992 to October 2020 - March 2021 used to generate relative anomaly plots over the storm season. This dataset is extended with preliminary data for 2024 from the same source but which has not yet been subjected to full quality control. The number of stations used to generate the gridded data varies from year to year, but currently consists of approximately 500 stations over Ireland. Further information on the preparation of these datasets can be found in (Coonan et al., 2024).

GISTEMP

As a measure of anthropogenic climate change we use the (low-pass filtered) global mean surface temperature (GMST), where GMST is taken from the National Aeronautics and Space Administration (NASA) Goddard Institute for Space Science (GISS) surface temperature analysis (GISTEMP, Hansen et al., 2010 and Lenssen et al. 2019).

2.2 Model and experiment descriptions

We use two types of model ensembles from climate modelling experiments using very different framings (Philip et al., 2020): The sea surface temperature (SST) driven global atmosphere-only circulation model ensemble HadGEM3-A, and the CMIP6 multi-model global coupled ocean-atmosphere circulation models. These two ensembles therefore provide a single-model with multiple members and conditioned on observed SSTs ensemble and a multi-model ensemble respectively.

Daily near surface wind speed at 10m and precipitation model diagnostics are used to derive the SSI and precipitation metrics respectively, monthly near surface 2m temperature and mean sea level pressure are used to derive the GMST and NAO indices for each model

(i) HadGEM3-A

The Met Office attribution system is described in Ciavarella et al. (2018). This is a system designed for the probabilistic attribution of extreme weather and climate events. It utilises a 60 km resolution version of the Hadley Centre atmospheric and land model with boundary conditions from observed Sea Surface Temperature (SST) and Sea Ice Concentration (SIC) taken from the HadISST1 dataset (Rayner et al. 2003). Well mixed Greenhouse Gas (GHG) concentrations are prescribed as annual values from the CMIP5 scenario data using historical values up to 2005 and following the RCP4.5 scenario from 2005 to present. Aerosols and Ozone are prescribed as CMIP5 recommended monthly values (Christidis et al. 2013) and land use prescribed decadally. Additionally natural forcings include solar irradiance and volcanic activity. The model is able to represent North Atlantic weather regimes and weather patterns associated with extreme temperature and precipitation (Vautard et al. 2018). In this analysis we use an ensemble of 15 members using a stochastic physics scheme as described in Ciavarella et al. (2018) spanning a period from 1961 to present.

(ii) CMIP6

This consists of simulations from 10 participating models accessible for this study. The models have varying resolutions and complexity. For more details on CMIP6, please see Eyring et al., (2016). For all simulations, the period 1850 to 2015 is based on historical simulations, while the SSP2-4.5 scenario ('middle of the road') is used for the remainder of the 21st century. Future analysis would benefit from utilising a larger ensemble of CMIP6 contributing models and further exploration of individual model ensembles.

2.3 Storm Severity Index

The SSI utilised is defined in equation (1) below.

$$SSI = \sum_{t=1}^{T} \sum_{k=1}^{K} \left[\left(max(0, \frac{v_{k,t}}{v_k^{98}} - 1) \right)^3 \cdot A_k \right] \quad (1)$$

Here the ratio is derived of the daily mean wind speed (v) at a height of 10m at location, k and time t and the 98th percentile for the years 1991-2020 of the daily mean wind speed (v^{98}) at location k. The max function ensures that only occurrences of wind speed above the 98th percentile for that location contribute to the SSI. The values are then summed across grid cells, with a normalised area weighting A_k to account for the latitudinal dependence of grid box area.

The SSI has been calculated over the domain shown in Fig. 2.3.1 below from daily mean 10m wind speed from the ERA5 reanalysis (Hersbach et al., 2020) and climate models described above. A region encompassing the UK and Ireland (red). The domain has also been further subdivided into a southern region largely containing England, Wales and Ireland, and a northern regime largely containing northern England, Scotland and Northern Ireland, with the separation line being located at 54N. Some additional sensitivity studies were conducted for larger domains (not shown), but the domain was chosen so that it was dominated by UK and Ireland land.

Figure 2.3.1: Map showing regions used to define wind indices in this analysis.

Region	Southwest Corner	Northeast Corner
UKIre domain (red)	(11W, 50N)	(2E, 61N)
South domain (red below --)	(11W, 50N)	(2E, 54N)
North domain (red above --)	(11W, 54N)	(2E, 61N)

Table 2.3.1. Definitions of the extent of each domain.

A comparison of the SSI indices has been made against alternative storm classifications to investigate the sensitivity of the subsequent attribution assessment to the choice of index. These are a count of the number of land stations in the UK observing network recording 10 m wind gusts in excess of 40, 50, and 60 knots (74, 92.6, 111.1 km/h respectively), which are thresholds that are routinely monitored and published in the annual State of UK Climate report (Kendon et al., 2023); and the Jenkinson gale index (Jenkinson & Collison, 1977; Jones et al., 1993) derived from NCEP reanalysis mean sea level pressure (Climatic Research Unit, 2024).

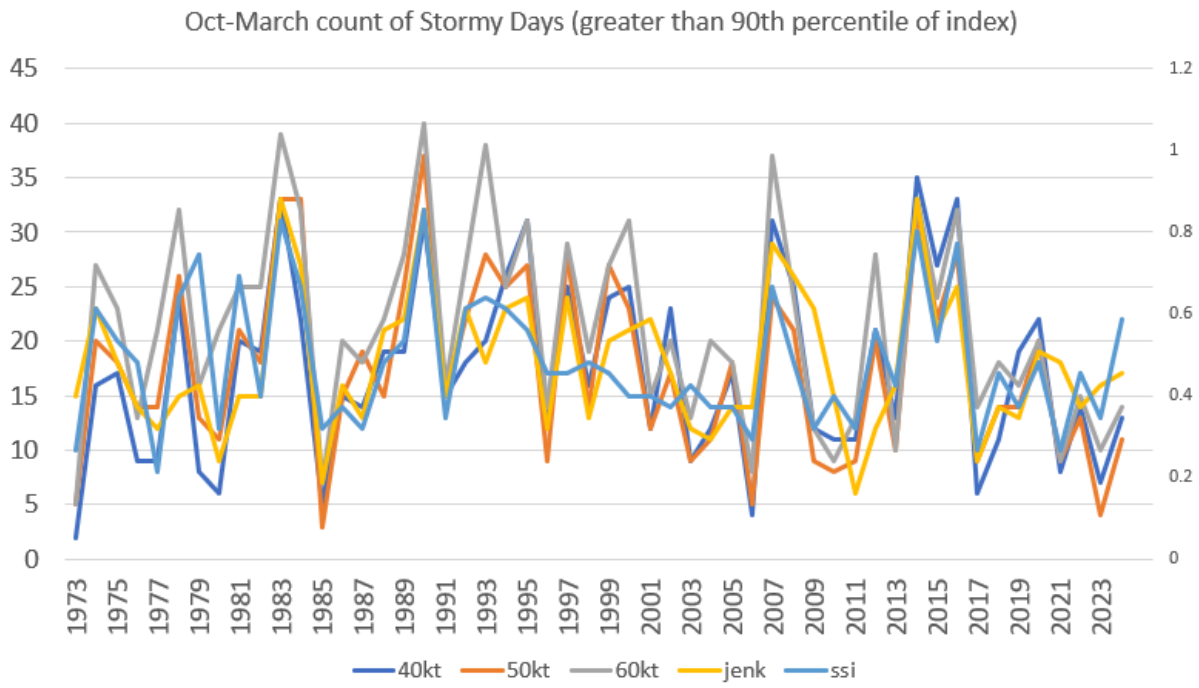

Figure 2.3.2. Comparison of indices that can be used to describe wind-based storm severity, showing the number of days per year exceeding the 90th percentile of the climatological distribution (1979-2020) of each index, a measure for the number of storm days per year. The year denotes the year at the end of the Oct-Mar season.

A comparison of the number of storm days defined by exceeding the 90th percentile of different indices is shown in Figure 2.3.2. This shows the broad consistency between these metrics for inter-annual and decadal variability in frequency of stormy days. The SSI was chosen for this study as it has a high correlation with station based surface wind metrics, and the NAO, and as the cube of wind speed it is designed to reflect potential damage of high wind.

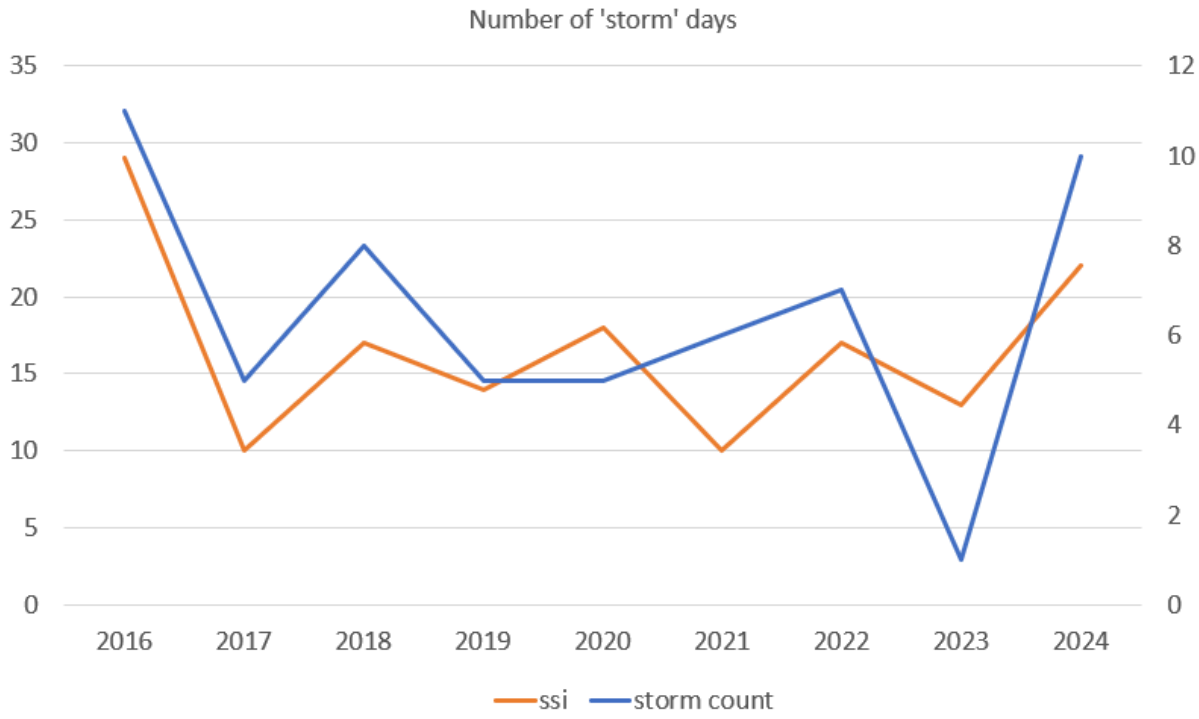

Figure 2.3.3 Comparison of number of storm days based on (orange and left hand axis) exceeding the 90th percentile of SSI for the UKIre domain and (blue and right hand axis) storms officially named by the storm naming partnership.

The storm days derived by the SSI is compared to the number of officially named storms in Figure 2.3.3 for the October to March periods from 2015/16 to 2023/24. The series of named storms is short and has evolved over this time, so is not in isolation a reliable climate metric for identifying trends. However for this short record there is correlation between the two series (coefficient 0.75). We can also evaluate hits and misses using the SSI. Over this period there were a total of 60 named storms in the October to March period. We associate an SSI storm day with a named storm if it occurs within 1 day of the documented dates (Met Office storm centre). 51 of the 60 storms had at least one day meeting the SSI criteria in at least one of the UKIre, north or south region. Approximately 45% of SSI days above the 90th percentile were associated with a named storm. Alternative thresholds were explored (not shown) and the 90th percentile determined to be a suitable balance between hit rate relative to named storms, and the total number of days identified. The storm naming scheme for the UK includes impact assessment within a risk framework so it is not expected that any objective climate index will perfectly represent named storms, but the comparison here demonstrates a good association between the SSI index and named storms.

In the analyses, we have determined the number of days exceeding the 90th percentile along with the sum of SSI on storm days through each season. The average SSI is then taken as the SSI sum divided by the number of stormy days within a given Oct-Mar season. Likewise, the average precipitation on stormy days is taken as the sum of precipitation on stormy days divided by the number of stormy days.

Figure 2.3.4 illustrates the method for storm Babet, where it can be seen which areas within the study domain contribute to the SSI on stormy days, and the same for precipitation (note that only daily

precipitation greater than 20 mm/dy is plotted in the figure for clarity, and ERA5 precipitation has been used instead of the Meteorological institutes' gridded precipitation products to show precipitation also outside of the study domain).

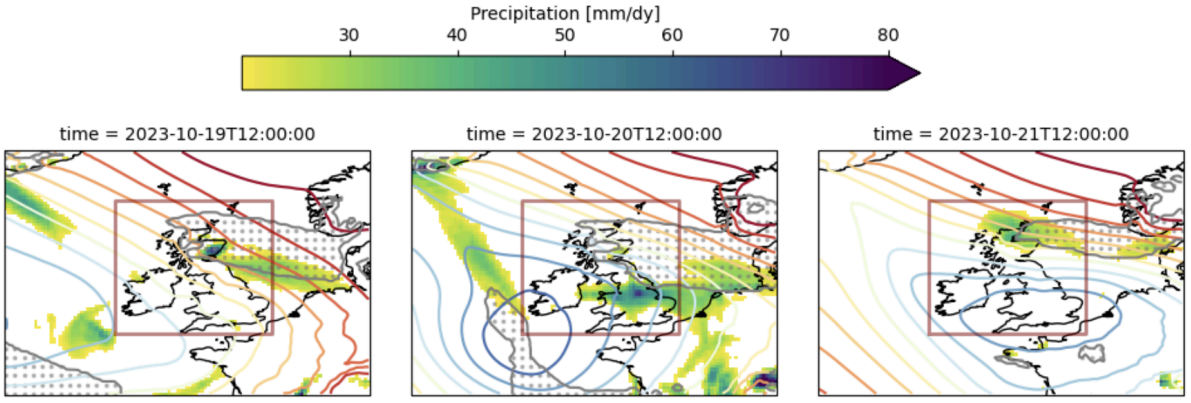

Figure 2.3.4 The passage of storm Babet from 19 October 2023 (left) to 21 October 2023 (right), shown in SLP (contours, every 4 mbar, with shading from blue (low pressure) to red (high pressure)), precipitation greater than 20 mm/day (background shading, colorbar) and region meeting SSI criterion, i.e. winds in excess of the 98th percentile of daily mean wind speed of years 1991-2020 (contoured in grey, with stippling for SSI>0). All three days classify as stormy days. Study region UKIre is shown as a box surrounding the UK and Ireland. Data: ERA5.

2.4 North Atlantic Oscillation Index

The North Atlantic Oscillation within ERA5 and the climate model analyses is calculated as the difference in the Mean Sea Level Pressure (MSLP) between two boxes located around Iceland (25W-16W, 63N-70N) and the Azores (28W-20W, 36N-40N) consistent with Dunstone et al. (2016). The normalised NAO series is averaged through the extended winter season October to March.

2.5 Statistical methods

In this analysis we analyse time series from the UKIre, North and South regions (see Fig. 2.3.1 and table 2.3.1) covering the UK and Ireland of mean SSI and precipitation values on Oct-Mar stormy days and Oct-Mar total precipitation, where long records of observed data are available. Methods for observational and model analysis and for model evaluation and synthesis are used according to the World Weather Attribution Protocol, described in Philip et al. (2020), with supporting details found in van Oldenborgh et al. (2021), Ciavarella et al. (2021) and here.

The analysis steps include: (i) trend calculation from observations; (ii) model validation; (iii) multi-method multi-model attribution and (iv) synthesis of the attribution statement.
We calculate the return periods, Probability Ratio (PR; the factor-change in the event's probability) and change in intensity (ΔI, the difference in magnitude of the metric between two reference states) of the event under study in order to compare the climate of now and the climate of the past, defined respectively by the GMST values of now and of the pre-industrial past (1850-1900, based on the Global Warming Index). For each metric that is studied we choose an appropriate distribution to describe the behaviour of the metric. Covariates are used to describe how the distribution changes

with other factors, here the GMST and the NAO index are selected as relevant covariants. These are factored into the statistical fit parameters as explained below in Section 2.5.1. The distributions and covariates selected are as follows. To statistically model the event under study, we use for stormy-day SSI a log-Normal that shifts with the covariate (GMST, NAO index), for stormy-day precipitation a Normal distribution that scales with the covariate (GMST, NAO index), and for Oct-Mar total precipitation a Normal distribution that scales with the covariate (GMST, NAO index). Note that (i) for distributions that shift with the covariate, the variance is held constant and ΔI is expressed as an absolute change in magnitude and is independent of the return period, and (ii) for distributions that scale with the covariate, the dispersion (mean/variance) is constant and ΔI is expressed as a relative change in percent and as such is also independent of the return period. In this study, a log-Normal distribution has been used with shift for the SSI metric. Results are subsequently transformed back to original units (to SSI from log(SSI)) where the ΔI is consequently transformed from an absolute to a relative measure and is expressed in percentage change. See the next paragraph for more details on the multivariate analysis. Next, results from observations and models that pass the validation tests are synthesised into a single attribution statement.

2.5.1 Statistical modelling of the combined effect of GMST and NAO

As noted in Section 1 storminess and associated precipitation over Northwestern Europe is known to be influenced by natural modes of variability, particularly the NAO.

In order to examine the effect of the NAO on rainy-season precipitation alongside that of increasing GMST, we extend the nonstationary model to accommodate an additional covariate. The variable of interest, X, is assumed to follow a normal distribution in which the location and scale parameters vary with both GMST and NAO:

$$X \sim N(\mu, \sigma \mid \mu_0,\ \sigma_0, \alpha, \beta,\ T,\ I),$$

where X denotes the variable of interest; T is the smoothed GMST, I is the NAO index, μ_0 and σ_0 are the mean and variance parameters of the nonstationary distribution and α, β are the trends due to GMST and NAO, respectively. As a result, the location and scale of the distribution have a different value in each year, determined by both the GMST and NAO states. Maximum likelihood estimation is used to estimate the model parameters, with

$$\mu = \mu_0 exp\left(\frac{\alpha T + \beta I}{\mu_o}\right) \quad \text{and} \quad \sigma = \sigma_0 exp\left(\frac{\alpha T + \beta I}{\mu_o}\right) \qquad (1)$$

$$\mu = \mu_0 + \alpha T + \beta I \quad \text{and} \quad \sigma = \sigma_0. \qquad (2)$$

Formulation (1) reflects the Clausius Clapeyron relation, which implies that precipitation scales exponentially with temperature (Trenberth et.al., 2003, O'Gorman and Schneider 2009), and so that precipitation will scale exponentially with the strength of the NAO index. Formulation (2) reflects the direct shifting of the log-Normal SSI. Under these models, the effects of GMST and the NAO index are assumed to be independent of one another, so that the change in intensity due to GMST is unaffected by the change in intensity due to the NAO phase. This is a reasonable assumption given that a possible link between NAO and GMST is not clear; a slight increase in NAO (i.e. towards more stormy conditions in northern Europe) has been shown on average in a warming climate (McKenna

and Maycock, 2022), but there are differences between how the NAO is projected to evolve in different climate models (McSweeney and Thornton, 2020).

2.5.2 Estimation of return periods

Extra care must be taken when reporting and interpreting return periods that depend on more than one covariate. Typically, WWA reports estimated return periods for the event of interest under current climatic conditions: in this case, with the GMST fixed at the 2023 level. In this study, there are two covariates to consider: the GMST and NAO index. By fixing both NAO and the GMST at their 2023 levels, we can estimate the return period of the 2023/24 event in the current climate and in the current NAO state. Mathematically, this return period is written as

$$1 / P(X > x_{2024} \mid T = t_{2024}, I = i_{2024}),$$

where x_{2023} is the 2023/24 value of observed precipitation; t_{2024} denotes the 2023/24 GMST; and i_{2024} denotes the mean of the NAO index from Oct2023-Mar2024. Altogether, the expression in brackets gives the probability that X will exceed x_{2024}, given that $T = t_{2024}$ and $I = i_{2024}$; inverting this probability gives us an expected return period, in years.

However, this return period only tells us the probability of experiencing a similar event under current NAO conditions and current warming levels. In order to understand how frequently such an event is actually likely to occur, we must account for the fact that the NAO is not often in the same phase observed in 2023/24. To do this, we evaluate the return period over all states of the NAO that have been recorded since 1960 (the period covered by both the observations and the models). This is done by first averaging the probability of exceeding x_{2024} over all recorded values of i_{2024} during this period, then inverting to obtain the return period:

$$1 / \sum_{y=1960}^{2024} P(X > x_{2024} \mid T = t_{2024}, I = i_y).$$

2.5.3 Defining the NAO state in climate models

The multi-method multi-model attribution step of the WWA protocol involves estimating, for each climate model, the effective return level of a 1-in-*n*-year event under the current climate state, and estimating the expected change in likelihood and intensity of such an event after a specified change in the covariates. Because the smoothed GMST is generally monotonically increasing, the standard WWA approach is simply to take the model's 2024 GMST as a covariate and to estimate the expected magnitude of an *n*-year event. However, the factual climate in this study is defined by the 2024 GMST and by the mean of the NAO index during the Oct-Mar rainy season. During the attribution step, the NAO index derived from the climate model is standardised so that the subset from 1960-2023 has mean 0 and variance 1; the 'factual' climate is then defined as having the model's 2024 GMST and the 2023/24 observed value of the NAO index, standardised in the same way. This removes any potential biases in the results due to differences between the amplitude of the modelled NAO index and that observed.

3 Observational analysis: return period and trend

3.1 Analysis of SSI

To explore trends in recent storminess, we fitted SSI data for the UKIre region; to further explore how this might vary geographically, we also fitted it for the North region and the South region.

Figure 3.1.1 shows the time series of the number of stormy days per year. No clear trend emerges from these time series. This was also the same for the models studied, with models showing a mixed sign of trends (1960-2100, not shown). This is not studied further, but it is incorporated in the stormy day SSI and precipitation statistics, which are sums normalised by the number of stormy days.

Figure 3.1.2 shows, for the three regions, the fitted model for average SSI on stormy days against the GMST covariate with the NAO covariate fixed at its mean NAO level and against the NAO covariate with the GMST covariate fixed at its mean GMST level, as well as the modelled changes in return levels due to a 1.2°C change in GMST from the pre-industrial to the current climate and due to the current NAO compared to an NAO value index of zero. All three regions show a trend with respect to both the GMST and the NAO covariate. We give the results below and in the remainder of this paper as the best estimate with the values in brackets showing the 95% confidence interval. The trends α and β due to GMST and NAO (equations (1) and (2)), are 0.71 (0.50 to 1.04), 0.74 (0.47 to 1.19) and 0.63 (0.32 to 1.32) for GMST for UKIre, North and South respectively, and 1.29 (1.12 to 1.47), 1.26 (1.09 to 1.46) and 1.32 (1.05 to 1.67) for NAO for UKIre, North and South respectively. However, the current NAO value is very small. This means that even though the inclusion of the NAO covariate in the analysis explains the data better, the current NAO value did only marginally influence the SSI. Therefore we only report the analysis results for SSI with respect to the GMST rise of 1.2°C.

There is a decreasing trend in average SSI on stormy days wrt GMST in all three regions. The 2023/24 event is estimated to have a return period of 3.7 (2.2 to 7.6) years for the UKIre region. For regions North and South the return periods are 3.8 years (2.3 to 8.1 years) and 2.6 years (1.6 to 5.2 years) respectively. Because these are all relatively similar and to make comparison between the regions easier we use a return period of 4 years for the model analysis for all three regions. The change in intensity is also similar for the three regions: -33% (-56% to 4.5%) for UKIre, -31% (-59% to 23%) for North and -43% (-75% to 39%) South respectively. This means that although the SSI values have become lower, the change is not significant in the relatively short time series. Similarly, the Probability Ratios show a (non-significant) trend towards high SSI values becoming less likely: a factor of 0.51 (0.21 to 1.18) for UKIre, 0.57 (0.020 to 1.35) for North and 0.63 (0.27 to 1.32) for South respectively.

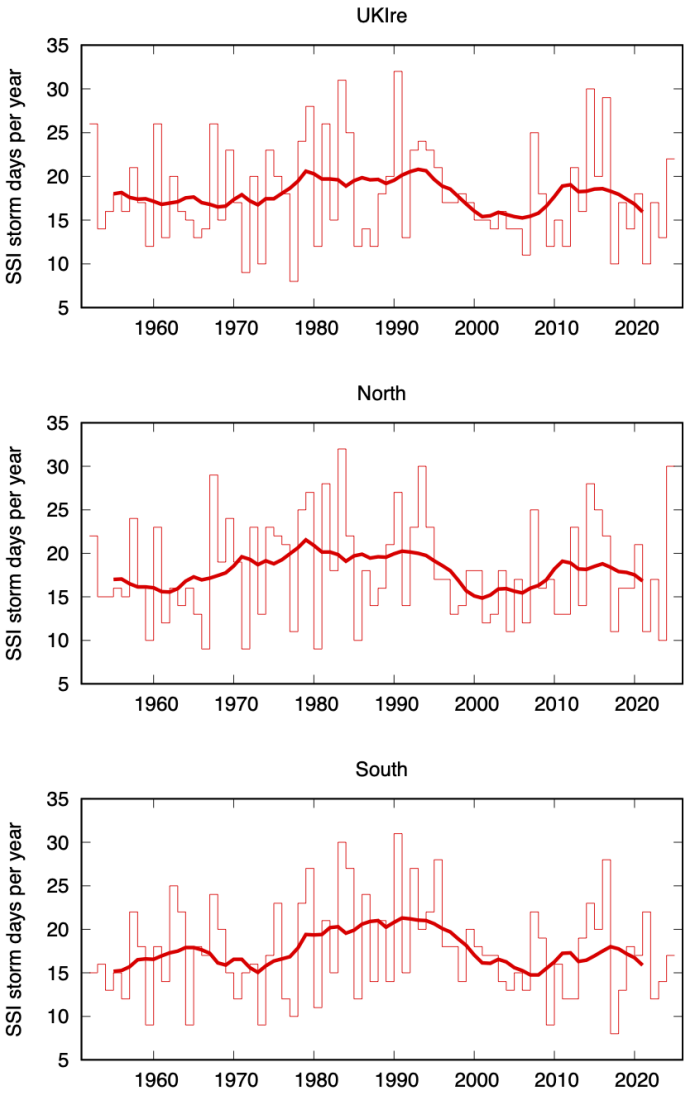

Figure 3.1.1 SSI stormy day count for the three regions (thin red) and 10-year running mean (thick red).

UKIre region

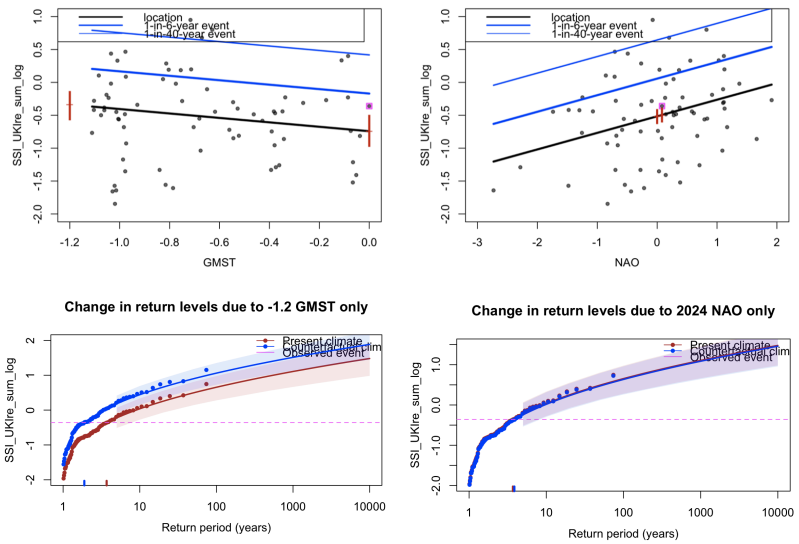

North region

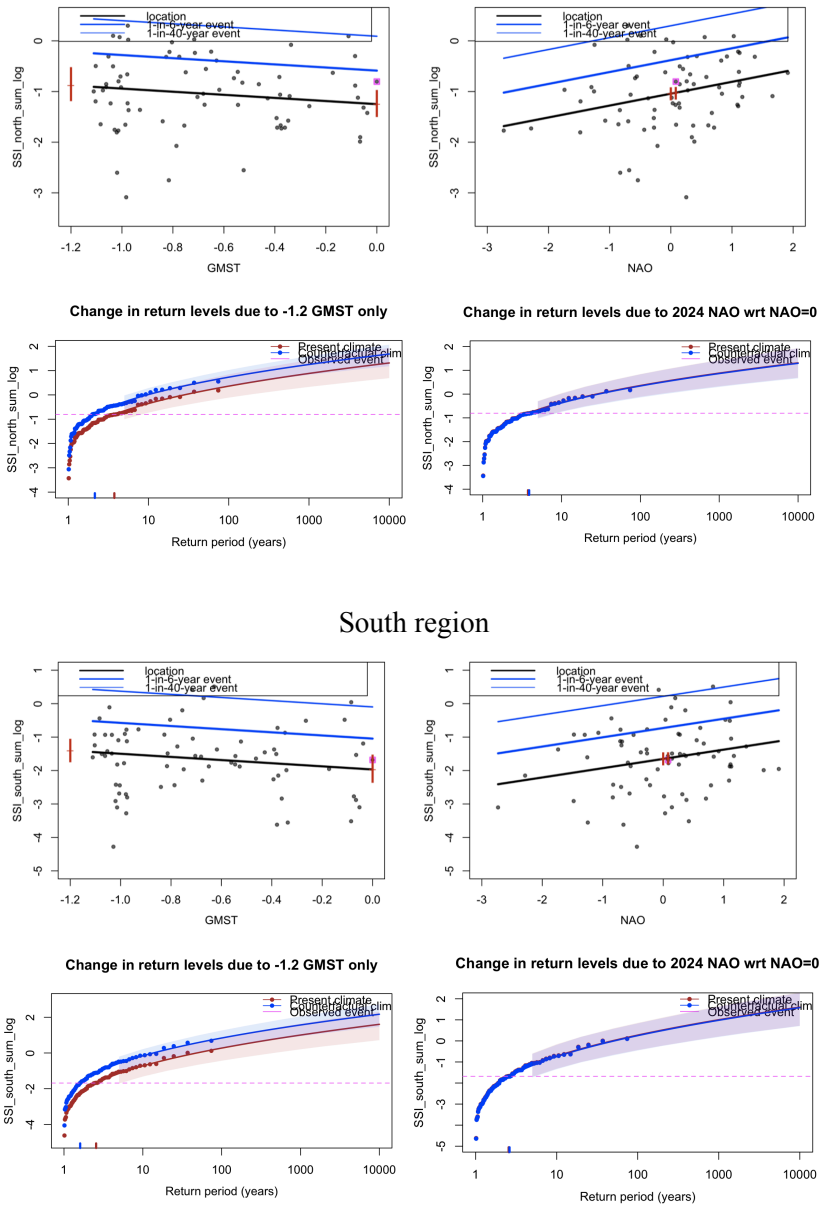

Fig 3.1.2 Average SSI in log scale for the UKIre region (top), North (centre) and South (bottom), showing trends with respect to GMST (left) and NAO (right) and corresponding return period plots for the changes in GMST and changes in NAO. In the trend plots, the thick black line denotes the location parameter of the fitted distribution, and the blue lines show estimated 6- and 40-year return levels. The 2023/24 observation is highlighted in magenta. Vertical lines show a bootstrapped confidence interval for the location parameter at the 2024 GMST and a 1.2°C cooler GMST (trend plots left); the 2023/24 NAO state and a neutral state (trend plots right). In the return period figures, shaded regions represent 95% confidence intervals obtained via a bootstrapping procedure. The dashed pink line shows the log-SSI value during the 2023/24 season. Red and blue ticks on the x axis indicate the best estimate return level of the 2023/24 season in the 2024 climate and 1.2°C cooler climate respectively (left) and the best estimate return level of the 2023/24 season in the 2023/24 NAO state and a neutral NAO state (right).

3.2 Analysis of precipitation on SSI-days

Because the differences in results for the SSI between the three regions are very small, we do not differentiate between the regions and only analyse precipitation on stormy days for the UKIre region.

Similar to Figure 3.1.1, Figure 3.2.1 shows the fitted model and changes in return period for the precipitation on SSI-days. Unlike the SSI analysis shown in Section 3.1, there is no trend in precipitation due to the NAO state, and the additional NAO covariate does not describe the data better than when using only GMST as a covariate. For simplicity we still use the same multivariate method as for the SSI. The return period and trend are the same when including the NAO or not (not shown).

There is an increasing trend in precipitation on stormy days wrt GMST. The 2023/24 event is estimated to have a return period of 5.77 (2.91 to 28.7) years for the UKIre region. For the model analysis we use a return period of 5 years. The change in intensity is 30.78% (6.02 to 56.5%) . This means that on SSI days, there is a significant increase in precipitation. Similarly, the Probability Ratio shows a significant trend of heavy precipitation becoming more likely: a factor of 41.4 (2.38 to 1650).

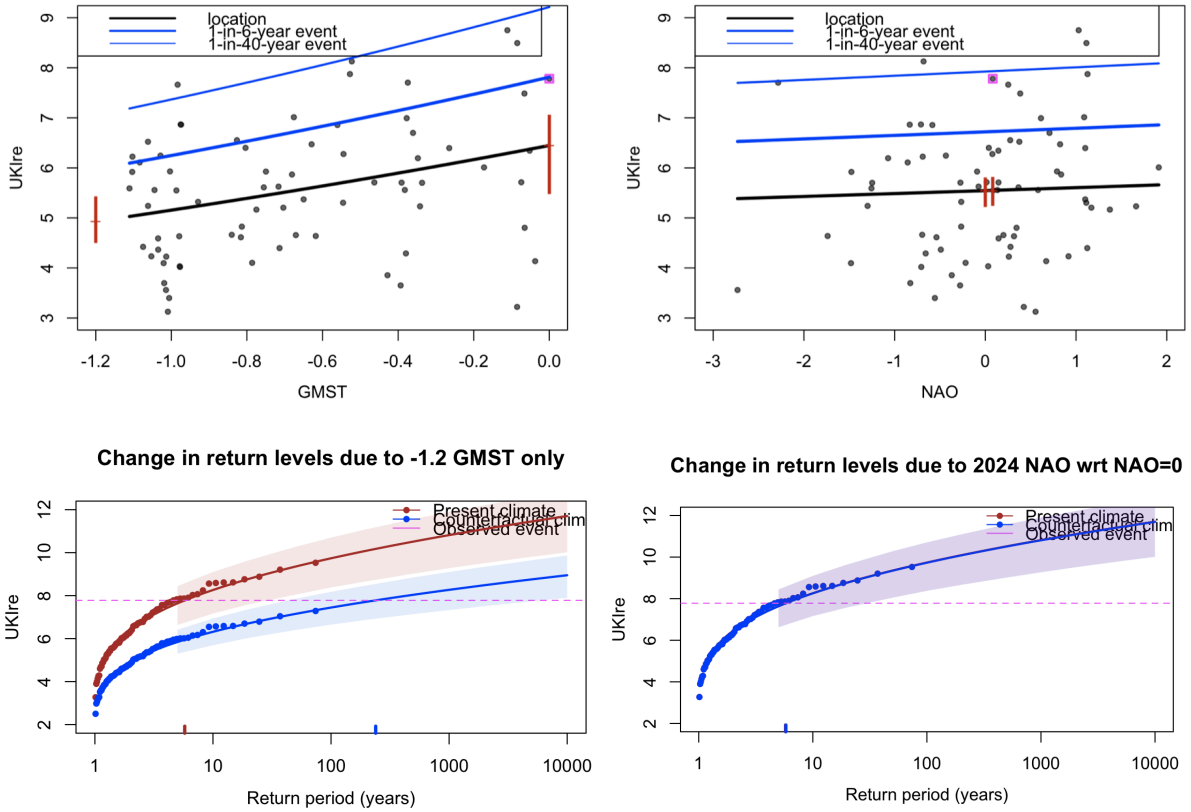

Fig 3.2.1 Similar to Fig. 3.1.1 but for average precipitation on stormy days for the UKIre region with a scale fit.

3.3 Analysis of seasonal precipitation

Because the impacts of seasonal precipitation were largest in the Southern domain, we focus the seasonal precipitation on region South only. Whereas for the UK and for Ireland the October 2023 - March 2024 precipitation sum was respectively the 2nd and 3rd highest on record, for our southern domain the 2023/24 season was the wettest in the observational time series (1951-2024).

Similar to the analysis of average precipitation on SSI days, there is no trend in precipitation due to the NAO state, and the additional NAO covariate does not describe the data better than when using

only GMST as a covariate. Again, for simplicity we still use the same multivariate method as for the SSI, but the return period and trend are the same when including the NAO or not (not shown).

There is an increasing trend in seasonal precipitation wrt GMST. The 2023/24 event is estimated to have a return period of 22.3 (7.7 to 211) years for the South region. For the model analysis we use a return period of 20 years. The change in intensity is 25% (9% to 410%). This means that there is a significant increase in seasonal precipitation. Similarly, the Probability Ratio shows a significant trend of heavy seasonal precipitation becoming more likely: a factor of 359 (8.8 to 46,800).

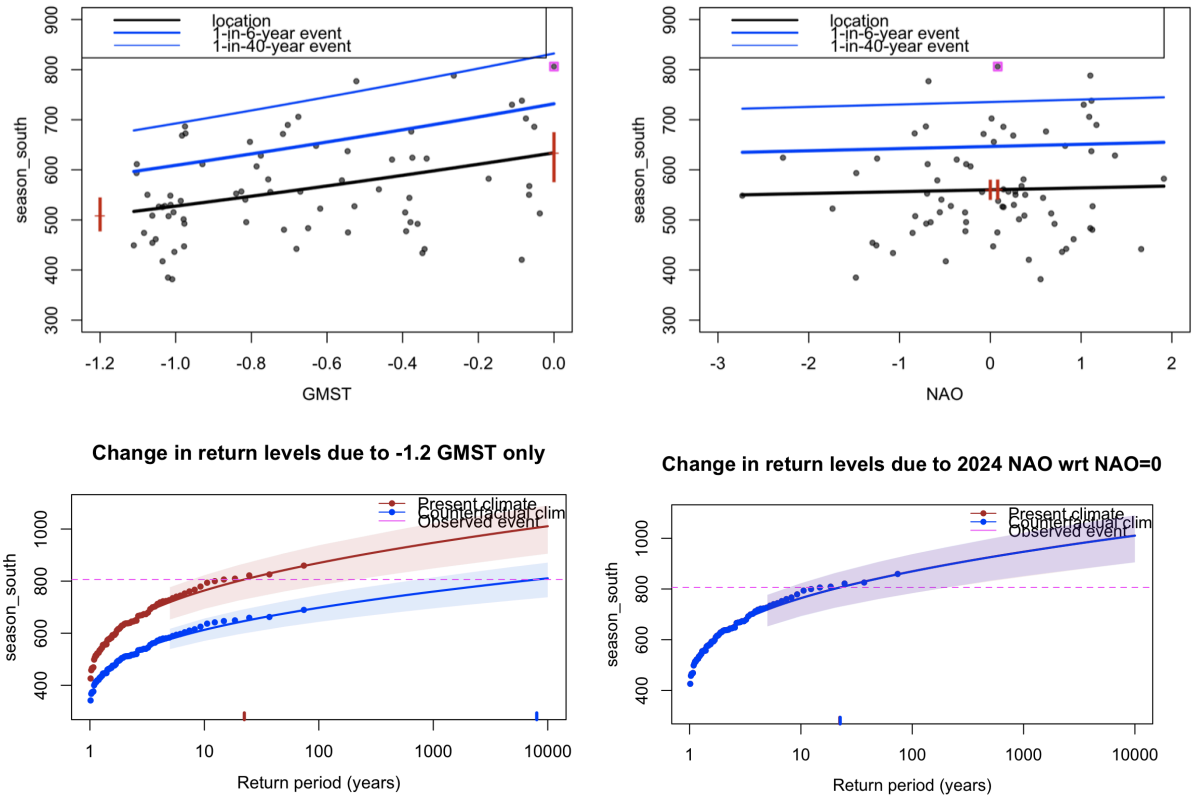

Fig 3.3.1 Similar to Fig. 3.1.1 but for the Oct-Mar precipitation accumulation for the South region with a scale fit.

3.4 Influence of other modes of natural variability

Atlantic Multidecadal Variability

The AMV – the decadal variability of Atlantic sea surface temperatures – is one factor that influences the NAO and the North Atlantic jet stream (Simpson et al., 2018). A study on storm Babet using analogues of circulation (Thompson et al., 2024, submitted to Weather and Climate Dynamics, preprint), showed that events similar to storm Babet are more likely during positive phases of the AMV, when the Atlantic is warmer than average. A higher chance of North East Scotland precipitation and stronger North Sea wind was found to be associated with the analogues of Babet, during September - November. We examined the influence of the AMV on Oct-Mar SSI in ERA5 but that explained less of the variance than the NAO (not shown) so we did not use AMV as a covariate in

the multivariate analysis. For precipitation, we find, that over the six months of Oct-Mar combined, there is no significant relationship of precipitation with the AMV and spatial maps of precipitation only show positive correlations in the east of the study domain during October (E-OBS, 1920-2022, not shown). At the beginning of the storm season, it is thus possible that the Atlantic Multidecadal Variability may influence precipitation over the study region, but it is not studied further here.

4 Model evaluation

In the subsections below we show the results of the model validation for the three indices and the different regions. Climate models are evaluated against observational data for their ability to capture the distribution of the fitted index - SSI, precipitation on SSI days and seasonal precipitation. The models are labelled as 'good' if the best estimate of each parameter of the statistical fit distribution (in this analysis, the parameters considered are the scale parameter or the dispersion of the fitted model, as appropriate, and the correlation between the index and the NAO) falls within the bounds estimated from the observations; 'reasonable' if the confidence interval for the model overlaps with the range estimated from the observations; or 'bad' if the ranges do not overlap. Models are also evaluated in terms of how well they represent the spatial and seasonal patterns of precipitation over the region. If the model is 'good' for all criteria, we give it an overall rating of 'good'. Overall we rate each model as 'reasonable' or 'bad', if it is rated 'reasonable' or 'bad', respectively, for at least one criterion.

4.1 Evaluation of SSI

Tables 4.1.1 to 4.1.3 show the results of the model evaluation for SSI for regions UKIre, North and South; because less than five models or ensemble members per model framing were evaluated as 'good', we also include the CMIP6 models and HadGEM3 ensemble members that were evaluated as 'reasonable' if the correlation with the NAO is 'good'. Where the statistical parameters evaluate as 'reasonable' and also the correlation with NAO is 'reasonable', this is noted in the tables as 'also NAO'. The exception is for domain South where 5 HadGEM3 ensemble members were labelled 'good', but we choose to use the same evaluation method for all three regions.

Table 4.1.1: *Evaluation of the climate models considered for attribution of SSI over the UKIre region. For each model, the best estimate of the shape parameters is shown, along with the correlation between SSI and the NAO index, and a 95% confidence interval for each, obtained via bootstrapping. The qualitative evaluation is shown in the right-hand column.*

Model / Observations	**Spatial pattern**	**Sigma**	**Shape parameter**	**Conclusion**
observations		0.592 (0.494 ... 0.662)	0.30 (0.087 ... 0.48)	
HadGEM3				
hadgem3_r1i1p10	good	0.731 (0.532 ... 0.890)	0.047 (-0.17 ... 0.26)	reasonable also NAO
hadgem3_r1i1p11	good	0.734 (0.526 ... 0.881)	0.36 (0.15 ... 0.53)	reasonable
hadgem3_r1i1p12	good	0.782 (0.550 ... 0.921)	0.30 (-0.092 ... 0.56)	reasonable

hadgem3_r1i1p13	good	0.797 (0.551 ... 0.966)	0.32 (0.066 ... 0.56)	reasonable
hadgem3_r1i1p14	good	0.742 (0.592 ... 0.823)	0.29 (0.066 ... 0.50)	reasonable
hadgem3_r1i1p15	good	1.07 (0.819 ... 1.23)	0.29 (0.085 ... 0.47)	bad
hadgem3_r1i1p1	good	1.01 (0.753 ... 1.19)	0.17 (-0.032 ... 0.37)	bad
hadgem3_r1i1p2	good	0.686 (0.521 ... 0.805)	0.33 (0.044 ... 0.58)	reasonable
hadgem3_r1i1p3	good	0.718 (0.523 ... 0.823)	0.25 (-0.023 ... 0.49)	reasonable
hadgem3_r1i1p4	good	0.743 (0.529 ... 0.894)	0.085 (-0.22 ... 0.35)	reasonable also NAO
hadgem3_r1i1p5	good	0.643 (0.498 ... 0.746)	0.18 (-0.043 ... 0.39)	good
hadgem3_r1i1p6	good	0.735 (0.495 ... 0.876)	0.25 (-0.067 ... 0.50)	reasonable
hadgem3_r1i1p7	good	0.757 (0.585 ... 0.867)	0.11 (-0.12 ... 0.35)	reasonable
hadgem3_r1i1p8	good	0.745 (0.583 ... 0.857)	0.47 (0.26 ... 0.65)	reasonable
hadgem3_r1i1p9	good	0.764 (0.564 ... 0.897)	0.13 (-0.10 ... 0.35)	reasonable
CMIP6				
ACCESS-CM2	good	0.651 (0.470 ... 0.789)	0.35 (0.20 ... 0.49)	good
ACCESS-ESM1-5	good	0.807 (0.624 ... 0.925)	0.053 (-0.10 ... 0.20)	reasonable also NAO
BCC-CSM2-MR	good	0.858 (0.677 ... 0.961)	0.21 (0.023 ... 0.40)	bad
CESM2	good	0.977 (0.713 ... 1.15)	0.20 (0.058 ... 0.34)	bad
CanESM5	good	0.860 (0.665 ... 0.979)	0.29 (0.15 ... 0.43)	bad
GFDL-ESM4	good	0.798 (0.621 ... 0.909)	0.11 (-0.046 ... 0.26)	reasonable
HadGEM3-GC31-LL	good	0.826 (0.639 ... 0.955)	0.26 (0.10 ... 0.42)	reasonable
IPSL-CM6A-LR	good	0.889 (0.636 ... 1.04)	0.23 (0.082 ... 0.38)	reasonable
MIROC6	reasonable	0.636 (0.438 ... 0.795)	0.27 (0.13 ... 0.41)	reasonable
MRI-ESM2-0	good	0.841 (0.630 ... 0.999)	0.31 (0.15 ... 0.45)	reasonable

Table 4.1.1: *Similar to Table 4.1.1 but for region South.*

Model / Observations	**Spatial pattern**	**Sigma**	**Shape parameter**	**Conclusion**
observations		0.684 (0.549 ... 0.809)	0.25 (0.065 ... 0.43)	
HadGEM3				
hadgem3_r1i1p10	good	1.12 (0.816 ... 1.32)	0.19 (0.022 ... 0.36)	bad
hadgem3_r1i1p11	good	1.04 (0.739 ... 1.22)	0.41 (0.24 ... 0.58)	reasonable
hadgem3_r1i1p12	good	0.978 (0.743 ... 1.13)	0.32 (0.0055 ... 0.54)	reasonable
hadgem3_r1i1p13	good	0.768 (0.566 ... 0.892)	0.45 (0.21 ... 0.64)	reasonable NAO

hadgem3_r1i1p14	good	0.890 (0.691 ... 0.998)	0.38 (0.14 ... 0.57)	reasonable
hadgem3_r1i1p15	good	1.10 (0.833 ... 1.29)	0.31 (0.092 ... 0.50)	bad
hadgem3_r1i1p1	good	1.03 (0.725 ... 1.25)	0.21 (-0.022 ... 0.42)	reasonable
hadgem3_r1i1p2	good	0.934 (0.707 ... 1.09)	0.26 (-0.0053 ... 0.51)	reasonable
hadgem3_r1i1p3	good	0.844 (0.626 ... 0.989)	0.26 (-0.0018 ... 0.49)	reasonable
hadgem3_r1i1p4	good	0.832 (0.567 ... 1.01)	0.14 (-0.095 ... 0.37)	reasonable
hadgem3_r1i1p5	good	0.999 (0.581 ... 1.32)	0.16 (-0.017 ... 0.36)	reasonable
hadgem3_r1i1p6	good	0.799 (0.568 ... 0.930)	0.078 (-0.23 ... 0.33)	good
hadgem3_r1i1p7	good	0.767 (0.600 ... 0.871)	0.16 (-0.080 ... 0.40)	good
hadgem3_r1i1p8	good	0.903 (0.721 ... 1.01)	0.36 (0.051 ... 0.59)	reasonable
hadgem3_r1i1p9	good	0.810 (0.626 ... 0.914)	0.055 (-0.16 ... 0.30)	reasonable also NAO
CMIP6				
ACCESS-CM2	good	0.880 (0.637 ... 1.04)	0.33 (0.16 ... 0.49)	reasonable
ACCESS-ESM1-5	good	0.954 (0.695 ... 1.12)	0.21 (0.062 ... 0.37)	reasonable
BCC-CSM2-MR	good	0.972 (0.703 ... 1.15)	0.27 (0.099 ... 0.44)	reasonable
CESM2	good	1.08 (0.772 ... 1.29)	0.15 (0.0030 ... 0.30)	reasonable
CanESM5	good	0.951 (0.666 ... 1.13)	0.33 (0.18 ... 0.48)	reasonable
GFDL-ESM4	good	0.890 (0.710 ... 0.988)	0.090 (-0.059 ... 0.24)	reasonable
HadGEM3-GC31-LL	good	1.14 (0.769 ... 1.43)	0.22 (0.059 ... 0.37)	reasonable
IPSL-CM6A-LR	good	0.922 (0.672 ... 1.07)	0.22 (0.071 ... 0.37)	reasonable
MIROC6	reasonable	0.944 (0.736 ... 1.08)	0.28 (0.13 ... 0.43)	reasonable >1x
MRI-ESM2-0	good	0.952 (0.691 ... 1.14)	0.29 (0.12 ... 0.44)	reasonable

Table 4.1.1: *Similar to Table 4.1.1 but for region North.*

Model / Observations	**Spatial pattern**	**Sigma**	**Shape parameter**	**Conclusion**
ERA5		0.955 (0.784 ... 1.08)	0.20 (-0.014 ... 0.39)	
HadGEM3				
hadgem3_r1i1p10	good	0.890 (0.671 ... 1.06)	-0.041 (-0.29 ... 0.23)	reasonable NAO
hadgem3_r1i1p11	good	1.03 (0.664 ... 1.26)	0.045 (-0.18 ... 0.27)	good
hadgem3_r1i1p12	good	1.17 (0.855 ... 1.34)	0.29 (-0.046 ... 0.53)	reasonable
hadgem3_r1i1p13	good	1.20 (0.800 ... 1.48)	0.11 (-0.11 ... 0.36)	reasonable
hadgem3_r1i1p14	good	1.15 (0.741 ... 1.43)	0.16 (-0.049 ... 0.42)	reasonable
hadgem3_r1i1p15	good	1.38 (1.03 ... 1.58)	0.25 (0.056 ... 0.45)	reasonable
hadgem3_r1i1p1	good	1.18 (0.911 ... 1.35)	0.10 (-0.12 ... 0.31)	reasonable
hadgem3_r1i1p2	good	0.943 (0.698 ... 1.13)	0.20 (-0.059 ... 0.45)	good
hadgem3_r1i1p3	good	1.07 (0.772 ... 1.26)	0.12 (-0.16 ... 0.39)	good
hadgem3_r1i1p4	good	1.19 (0.904 ... 1.37)	0.091 (-0.22 ... 0.37)	reasonable

hadgem3_r1i1p5	good	1.06 (0.815 ... 1.22)	0.028 (-0.19 ... 0.25)	good
hadgem3_r1i1p6	good	1.38 (0.717 ... 1.80)	0.38 (0.11 ... 0.55)	reasonable
hadgem3_r1i1p7	good	1.05 (0.824 ... 1.18)	0.24 (-0.041 ... 0.49)	good
hadgem3_r1i1p8	good	1.11 (0.722 ... 1.46)	0.42 (0.26 ... 0.62)	reasonable NAO
hadgem3_r1i1p9	good	1.11 (0.778 ... 1.36)	0.14 (-0.090 ... 0.39)	reasonable
CMIP6				
ACCESS-CM2	good	0.984 (0.667 ... 1.22)	0.22 (0.073 ... 0.35)	good
ACCESS-ESM1-5	good	0.926 (0.721 ... 1.05)	-0.036 (-0.19 ... 0.11)	reasonable, also NAO
BCC-CSM2-MR	good	1.15 (0.915 ... 1.28)	0.14 (-0.063 ... 0.31)	reasonable
CESM2	good	1.19 (0.911 ... 1.36)	0.23 (0.070 ... 0.38)	reasonable
CanESM5	good	1.17 (0.862 ... 1.39)	0.18 (0.033 ... 0.34)	reasonable
GFDL-ESM4	good	1.07 (0.697 ... 1.37)	0.036 (-0.12 ... 0.18)	good
HadGEM3-GC31-LL	good	0.986 (0.761 ... 1.10)	0.31 (0.13 ... 0.48)	good
IPSL-CM6A-LR	good	1.19 (0.802 ... 1.49)	0.26 (0.096 ... 0.43)	reasonable
MIROC6	reasonable	0.834 (0.634 ... 0.997)	0.13 (-0.012 ... 0.28)	reasonable
MRI-ESM2-0	good	1.08 (0.845 ... 1.23)	0.26 (0.097 ... 0.40)	reasonable

4.2 Evaluation of precipitation on SSI-days

Table 4.2 shows the results of the model evaluation for precipitation on SSI-days for region UKIre, North and South; because more than five HadGEM3 ensemble members were evaluated as ‘good’ , only 'good' HadGEM3 ensemble members were included in the final synthesis described in Section 5. For the CMIP6 ensemble, less than 5 models were evaluated as 'good' so we also include the 'reasonable' models. Models that were evaluated 'bad' for the evaluation on the SSI were also excluded from the synthesis.

Table 4.2.1: *Similar to Table 4.1.1 but for precipitation on SSI days.*

Model / Observations	**Seasonal cycle**	**Spatial pattern**	**Dispersion**	**Shape parameter**	**Conclusion**
observations			0.203 (0.169 ... 0.228)	0.12 (-0.13 ... 0.36)	
HadGEM3					
hadgem3_r1i1p10	good	good	0.201 (0.153 ... 0.230)	0.23 (0.0083 ... 0.43)	good
hadgem3_r1i1p11	good	good	0.202 (0.142 ... 0.244)	0.10 (-0.13 ... 0.33)	good
hadgem3_r1i1p12	good	good	0.184 (0.132 ... 0.219)	-0.11 (-0.38 ... 0.27)	reasonable
hadgem3_r1i1p13	good	good	0.196 (0.142 ... 0.233)	-0.17 (-0.44 ... 0.14)	reasonable
hadgem3_r1i1p14	good	good	0.200 (0.161 ... 0.230)	0.058 (-0.21 ... 0.33)	good
hadgem3_r1i1p15	good	good	0.184 (0.125 ... 0.220)	0.21 (-0.087 ... 0.47)	bad, SSI validation bad
hadgem3_r1i1p1	good	good	0.169 (0.132 ... 0.189)	0.056 (-0.16 ... 0.28)	bad, SSI validation bad

hadgem3_r1i1p2	good	good	0.152 (0.119 ... 0.174)	-0.13 (-0.32 ... 0.11)	reasonable
hadgem3_r1i1p3	good	good	0.168 (0.123 ... 0.197)	0.056 (-0.16 ... 0.30)	reasonable
hadgem3_r1i1p4	good	good	0.182 (0.138 ... 0.216)	-0.10 (-0.34 ... 0.13)	reasonable
hadgem3_r1i1p5	good	good	0.205 (0.154 ... 0.239)	0.11 (-0.10 ... 0.32)	good
hadgem3_r1i1p6	good	good	0.166 (0.120 ... 0.196)	0.40 (0.14 ... 0.59)	reasonable
hadgem3_r1i1p7	good	good	0.157 (0.117 ... 0.183)	0.14 (-0.13 ... 0.38)	reasonable
hadgem3_r1i1p8	good	good	0.181 (0.137 ... 0.215)	0.23 (-0.060 ... 0.47)	good
hadgem3_r1i1p9	good	good	0.171 (0.131 ... 0.195)	0.11 (-0.16 ... 0.38)	reasonable
CMIP6					
ACCESS-CM2	reasonable	good	0.155 (0.121 ... 0.183)	0.12 (-0.033 ... 0.27)	reasonable
ACCESS-ESM1-5	reasonable	good	0.136 (0.102 ... 0.157)	-0.051 (-0.21 ... 0.11)	bad, SSI validation bad
BCC-CSM2-MR	reasonable	good	0.141 (0.111 ... 0.160)	-0.15 (-0.32 ... 0.022)	bad, SSI validation bad
CESM2	reasonable	good	0.145 (0.108 ... 0.168)	0.16 (-0.027 ... 0.33)	bad, SSI validation bad
CanESM5	reasonable	bad	0.197 (0.157 ... 0.220)	-0.20 (-0.35 ... -0.040)	bad
GFDL-ESM4	reasonable	reasonable	0.163 (0.114 ... 0.197)	-0.098 (-0.27 ... 0.071)	reasonable
HadGEM3-GC31-LL	reasonable	good	0.150 (0.113 ... 0.174)	-0.0017 (-0.18 ... 0.17)	bad
IPSL-CM6A-LR	reasonable	good	0.125 (0.0956 ... 0.146)	-0.0012 (-0.20 ... 0.18)	bad, SSI validation bad
MIROC6	reasonable	good	0.202 (0.151 ... 0.242)	0.015 (-0.12 ... 0.14)	good
MRI-ESM2-0	reasonable	good	0.142 (0.107 ... 0.165)	-0.0066 (-0.17 ... 0.14)	bad, SSI validation bad

4.3 Evaluation of seasonal precipitation

Table 4.3 shows the results of the model evaluation for seasonal precipitation for region South; because more than five models and HadGEM3 ensemble members were evaluated as ‘good’ per framing, only 'good' models were included in the final synthesis described in Section 5. For CMIP6, only models that passed the evaluation of the distribution parameters as 'good' were included in the final synthesis described in Section 5, as all seasonal cycles were labelled 'reasonable'.

Table 4.3.1: *Similar to Table 4.1.1 but for seasonal precipitation in region South.*

Model / Observations	**Seasonal cycle**	**Spatial pattern**	**Dispersion**	**Shape parameter**	**Conclusion**
observations			0.160 (0.134 ... 0.176)	0.13 (-0.087 ... 0.35)	
HadGEM3					
hadgem3_r1i1p10	good	good	0.181 (0.127 ... 0.220)	0.29 (0.10 ... 0.46)	reasonable

hadgem3_r1i1p11	good	good	0.158 (0.121 ... 0.179)	0.096 (-0.17 ... 0.35)	good
hadgem3_r1i1p12	good	good	0.174 (0.121 ... 0.218)	0.28 (0.020 ... 0.49)	good
hadgem3_r1i1p13	good	good	0.159 (0.122 ... 0.185)	0.038 (-0.17 ... 0.26)	good
hadgem3_r1i1p14	good	good	0.150 (0.104 ... 0.190)	0.31 (0.018 ... 0.55)	good
hadgem3_r1i1p15	good	good	0.184 (0.143 ... 0.210)	0.28 (0.053 ... 0.51)	reasonable
hadgem3_r1i1p1	good	good	0.157 (0.124 ... 0.180)	0.13 (-0.080 ... 0.32)	good
hadgem3_r1i1p2	reasonable	good	0.173 (0.122 ... 0.206)	0.21 (-0.0039 ... 0.43)	reasonable
hadgem3_r1i1p3	good	good	0.157 (0.110 ... 0.181)	0.26 (0.027 ... 0.48)	good
hadgem3_r1i1p4	good	good	0.176 (0.128 ... 0.204)	0.16 (-0.10 ... 0.40)	good
hadgem3_r1i1p5	good	good	0.164 (0.123 ... 0.194)	0.28 (0.011 ... 0.54)	good
hadgem3_r1i1p6	good	good	0.188 (0.125 ... 0.251)	0.35 (0.059 ... 0.57)	reasonable
hadgem3_r1i1p7	good	good	0.126 (0.0847 ... 0.161)	0.18 (-0.10 ... 0.38)	reasonable
hadgem3_r1i1p8	good	good	0.176 (0.135 ... 0.208)	0.38 (0.18 ... 0.57)	reasonable
hadgem3_r1i1p9	good	good	0.176 (0.128 ... 0.212)	-0.030 (-0.27 ... 0.21)	reasonable
CMIP6					
ACCESS-CM2	reasonable	good	0.123 (0.0803 ... 0.150)	0.18 (-0.0092 ... 0.34)	reasonable >1x
ACCESS-ESM1-5	reasonable	good	0.133 (0.103 ... 0.153)	0.22 (0.046 ... 0.37)	reasonable >1x
BCC-CSM2-MR	reasonable	good	0.143 (0.112 ... 0.158)	0.081 (-0.093 ... 0.25)	reasonable
CESM2	reasonable	good	0.139 (0.105 ... 0.165)	0.18 (0.013 ... 0.34)	reasonable
CanESM5	reasonable	bad	0.125 (0.0953 ... 0.144)	-0.18 (-0.33 ... -0.026)	bad
GFDL-ESM4	reasonable	reasonable	0.124 (0.0991 ... 0.141)	0.016 (-0.16 ... 0.19)	reasonable >1x
HadGEM3-GC31-LL	reasonable	good	0.138 (0.110 ... 0.155)	0.12 (-0.048 ... 0.27)	reasonable
IPSL-CM6A-LR	reasonable	good	0.112 (0.0876 ... 0.127)	-0.027 (-0.20 ... 0.14)	bad
MIROC6	reasonable	good	0.147 (0.107 ... 0.176)	0.00084 (-0.17 ... 0.16)	reasonable
MRI-ESM2-0	reasonable	good	0.145 (0.110 ... 0.171)	0.20 (0.043 ... 0.34)	reasonable

5 Multi-method multi-model attribution

The subsections below show Probability Ratios and change in intensity ΔI for models that passed the evaluation and also includes the values calculated from the fits with observations.

5.1 Results SSI

Table 5.1.1: *Event magnitude, probability ratio and relative change in intensity for a 4-year SSI event over region UKIre for observational datasets and each model that passed evaluation: (a) from the pre-industrial climate to the present and (b) from the present to 2°C above pre-industrial. Where data is not applicable (e.g. observations of the future), cells have been shaded grey.*

		past - present		**present - future**	
Model / Observations	**Threshold for return period 4 yr (log-SSI)**	**Probability ratio PR [-]**	**Change in intensity ΔI [%]**	**Probability ratio PR [-]**	**Change in intensity ΔI [%]**
observations	-0.36026	0.51 (0.21 ... 1.1)	-33 (-56 ... 4.5)		
Hadgem3					
hadgem3_r1i1p11	-1.7	0.69 (0.13 ... 5.8)	-21 (-73 ... 1.4e+2)		
hadgem3_r1i1p12	-1.8	0.54 (0.13 ... 2.6)	-36 (-74 ... 76)		
hadgem3_r1i1p13	-1.8	0.54 (0.11 ... 2.6)	-36 (-78 ... 90)		
hadgem3_r1i1p14	-1.3	2.5 (0.41 ... 53)	63 (-42 ... 3.6e+2)		
hadgem3_r1i1p2	-1.6	0.99 (0.24 ... 5.7)	-0.49 (-53 ... 1.2e+2)		
hadgem3_r1i1p3	-1.7	0.52 (0.14 ... 2.1)	-36 (-73 ... 50)		
hadgem3_r1i1p5	-1.8	0.92 (0.22 ... 5.0)	-4.4 (-55 ... 92)		
hadgem3_r1i1p6	-1.7	0.43 (0.12 ... 2.7)	-48 (-85 ... 65)		
hadgem3_r1i1p7	-1.7	0.65 (0.16 ... 4.3)	-27 (-78 ... 1.3e+2)		
hadgem3_r1i1p8	-1.6	1.5 (0.27 ... 12)	22 (-48 ... 1.9e+2)		
hadgem3_r1i1p9	-1.3	4.1 (0.39 ... 1.1e+2)	99 (-36 ... 5.5e+2)		
Hadgem3 ensemble		0.75 (0.47 ... 1.3)	-9.6 (-32 ... 21)		
CMIP6					
ACCESS-CM2	-3.5	0.60 (0.13 ... 1.7)	-25 (-59 ... 38)	0.95 (0.67 ... 1.2)	-3.2 (-16 ... 15)
GFDL-ESM4	-2.6	0.56 (0.20 ... 1.4)	-33 (-64 ... 30)	0.98 (0.62 ... 1.3)	-1.2 (-23 ... 26)
HadGEM3-GC31-LL	-3.5	1.2 (0.50 ... 2.3)	12 (-27 ... 70)	0.64 (0.40 ... 0.88)	-18 (-28 ... -5.5)
IPSL-CM6A-LR	-3.6	1.1 (0.34 ... 3.3)	7.2 (-47 ... 1.1e+2)	1.0 (0.72 ... 1.3)	0.24 (-17 ... 22)
MIROC6	-2.8	0.38 (0.17 ... 1.0)	-49 (-73 ... 0.20)	0.47 (0.15 ... 0.87)	-32 (-50 ... -8.9)

MRI-ESM2-0	-2.7	0.70 (0.20 ... 2.0)	-22 (-62 ... 58)	0.83 (0.54 ... 1.1)	-11 (-27 ... 6.9)

Table 5.1.2: *Similar to Table 5.1.1 but for region North*

		past - present		**present - future**	
Model / Observations	**Threshold for return period 4 yr (log-SSI)**	**Probability ratio PR [-]**	**Change in intensity ΔI [%]**	**Probability ratio PR [-]**	**Change in intensity ΔI [%]**
observations	-0.80402578	0.57 (0.20 ... 1.3)	-31 (-59 ... 23)		
HadGEM3					
hadgem3_r1i1p11	-2.3	0.70 (0.16 ... 3.3)	-26 (-76 ... 1.4e+2)		
hadgem3_r1i1p12	-2.1	1.2 (0.21 ... 12)	15 (-63 ... 2.8e+2)		
hadgem3_r1i1p14	-1.8	13 (1.2 ... 3.8e+2)	2.5e+2 (7.5 ... 9.9e+2)		
hadgem3_r1i1p1	-2.7	0.38 (0.083 ... 1.5)	-68 (-93 ... 45)		
hadgem3_r1i1p2	-2.3	0.44 (0.14 ... 1.6)	-52 (-84 ... 42)		
hadgem3_r1i1p3	-2.3	0.69 (0.13 ... 5.0)	-24 (-80 ... 1.4e+2)		
hadgem3_r1i1p4	-2.2	1.7 (0.25 ... 21)	40 (-60 ... 3.4e+2)		
hadgem3_r1i1p5	-2.4	0.64 (0.14 ... 3.4)	-30 (-82 ... 1.1e+2)		
hadgem3_r1i1p6	-2.0	2.1 (0.27 ... 70)	56 (-59 ... 5.0e+2)		
hadgem3_r1i1p7	-2.0	1.8 (0.25 ... 22)	42 (-57 ... 3.7e+2)		
hadgem3_r1i1p8	-2.0	2.6 (0.33 ... 32)	77 (-46 ... 4.9e+2)		
Hadgem3 ensemble		0.87 (0.40 ... 2.0)	5.5 (-42 ... 92)		
CMIP6					
ACCESS-CM2	-3.9	0.77 (0.23 ... 1.9)	-16 (-54 ... 62)	0.92 (0.68 ... 1.2)	-5.1 (-19 ... 12)
ACCESS-ESM1-5	-4.4	1.3 (0.48 ... 3.5)	18 (-40 ... 1.1e+2)	1.0 (0.68 ... 1.3)	2.3 (-21 ... 32)
BCC-CSM2-MR	-3.0	1.4 (0.46 ... 5.1)	28 (-39 ... 1.8e+2)	1.2 (0.77 ... 1.6)	14 (-18 ... 59)
CESM2	-3.4	0.42 (0.15 ... 0.87)	-61 (-84 ... -15)	0.86 (0.60 ... 1.1)	-13 (-35 ... 11)
CanESM5	-4.8	0.87 (0.34 ... 1.7)	-10 (-48 ... 50)	0.64 (0.40 ... 0.86)	-25 (-38 ... -10)
GFDL-ESM4	-3.0	1.0 (0.33 ... 3.3)	0.54 (-50 ... 1.1e+2)	1.2 (0.83 ... 1.6)	12 (-10 ... 38)
HadGEM3-GC31-LL	-4.4	0.71 (0.17 ... 1.5)	-27 (-70 ... 54)	0.68 (0.45 ... 0.88)	-24 (-36 ... -9.2)
IPSL-CM6A-LR	-4.2	0.97 (0.30 ... 2.8)	-2.4 (-54 ... 1.2e+2)	0.97 (0.68 ... 1.3)	-2.5 (-22 ... 23)
MRI-ESM2-0	-3.1	0.86 (0.27 ... 2.5)	-10 (-58 ... 89)	0.82 (0.52 ... 1.2)	-12 (-31 ... 12)

Table 5.1.3: *Similar to Table 5.1.1 but for region South*

		past - present		present - future	
Model / Observations	**Threshold for return period 4 yr (log-SSI)**	**Probability ratio PR [-]**	**Change in intensity ΔI [%]**	**Probability ratio PR [-]**	**Change in intensity ΔI [%]**
ERA5	-1.68298416	0.63 (0.27 ... 1.3)	-43 (-75 ... 40)		
HadGEM3					
hadgem3_r1i1p11	-2.4	0.99 (0.16 ... 20)	-0.59 (-82 ... 4.4e+2)		
hadgem3_r1i1p12	-3.0	0.43 (0.14 ... 1.5)	-64 (-91 ... 52)		
hadgem3_r1i1p13	-2.6	0.71 (0.16 ... 4.3)	-28 (-83 ... 2.1e+2)		
hadgem3_r1i1p14	-2.1	1.3 (0.25 ... 13)	22 (-70 ... 4.7e+2)		
hadgem3_r1i1p15	-2.6	0.60 (0.17 ... 2.6)	-46 (-90 ... 1.6e+2)		
hadgem3_r1i1p1	-2.5	0.73 (0.12 ... 4.9)	-29 (-88 ... 3.1e+2)		
hadgem3_r1i1p2	-2.4	3.5 (0.52 ... 39)	1.1e+2 (-31 ... 6.0e+2)		
hadgem3_r1i1p3	-2.6	0.56 (0.17 ... 1.9)	-43 (-81 ... 73)		
hadgem3_r1i1p4	-2.1	2.1 (0.42 ... 23)	78 (-53 ... 6.3e+2)		
hadgem3_r1i1p5	-2.7	0.81 (0.19 ... 3.8)	-18 (-79 ... 1.6e+2)		
hadgem3_r1i1p6	-3.1	0.27 (0.092 ... 0.72)	-92 (-99 ... -36)		
hadgem3_r1i1p7	-2.8	0.46 (0.15 ... 1.7)	-57 (-89 ... 65)		
hadgem3_r1i1p9	-2.0	6.4 (0.66 ... 2.0e+2)	2.3e+2 (-21 ... 1.3e+3)		
Hadgem3 ensemble		0.67 (0.32 ... 1.4)	-16 (-68 ... 1.2e+2)		
CMIP6					
ACCESS-CM2	-3.9	0.70 (0.17 ... 2.0)	-26 (-71 ... 88)	0.98 (0.71 ... 1.3)	-2.1 (-21 ... 28)
BCC-CSM2-MR	-3.0	3.5 (0.95 ... 15)	1.5e+2 (-3.5 ... 5.2e+2)	1.7 (1.3 ... 2.3)	67 (24 ... 1.3e+2)
CESM2	-2.9	0.90 (0.31 ... 3.2)	-10 (-67 ... 1.5e+2)	0.92 (0.62 ... 1.3)	-8.3 (-33 ... 28)
CanESM5	-5.6	0.61 (0.23 ... 1.1)	-42 (-70 ... 16)	0.86 (0.65 ... 1.1)	-16 (-34 ... 7.7)
GFDL-ESM4	-3.6	0.35 (0.14 ... 0.82)	-72 (-89 ... -20)	0.80 (0.47 ... 1.1)	-23 (-46 ... 13)
HadGEM3-GC31-LL	-3.7	1.5 (0.56 ... 3.0)	35 (-29 ... 1.4e+2)	0.76 (0.49 ... 1.1)	-15 (-30 ... 3.9)
IPSL-CM6A-LR	-4.0	0.89 (0.26 ... 2.6)	-9.8 (-64 ... 1.2e+2)	0.92 (0.61 ... 1.2)	-6.2 (-26 ... 19)
MIROC6	-3.5	0.36 (0.14 ... 0.89)	-60 (-83 ... -8.1)	0.41 (0.15 ... 0.74)	-42 (-59 ... -19)
MRI-ESM2-0	-3.4	0.67 (0.17 ... 1.8)	-31 (-75 ... 73)	0.88 (0.59 ... 1.1)	-11 (-29 ... 15)

5.2 Results precipitation on SSI-days

Table 5.3.1: *Similar to Table 5.1.1 but for precipitation on SSI days.*

		past - present		present - future	
Model / Observations	**Threshold for return period 5 yr**	**Probability ratio PR [-]**	**Change in intensity ΔI [%]**	**Probability ratio PR [-]**	**Change in intensity ΔI [%]**
observations	9.898 mm/day	1.1e+2 (6.0 ... 1.1e+4)	35 (13 ... 58)		
HadGEM3					
hadgem3_r1i1p10	6.2 mm/day	0.43 (0.068 ... 1.9)	-12 (-33 ... 8.9)		
hadgem3_r1i1p11	6.9 mm/day	29 (0.36 ... 8.3e+3)	27 (-7.1 ... 60)		
hadgem3_r1i1p12	7.0 mm/day	3.2 (0.27 ... 1.5e+2)	12 (-12 ... 38)		
hadgem3_r1i1p14	6.6 mm/day	1.1 (0.14 ... 12)	1.5 (-18 ... 25)		
hadgem3_r1i1p4	6.0 mm/day	0.34 (0.12 ... 1.0)	-17 (-30 ... 0.11)		
hadgem3_r1i1p5	6.6 mm/day	0.74 (0.13 ... 5.3)	-3.9 (-24 ... 17)		
hadgem3_r1i1p8	6.6 mm/day	1.1 (0.15 ... 10)	0.93 (-19 ... 24)		
hadgem3_r1i1p9	7.0 mm/day	16 (0.47 ... 1.1e+3)	20 (-5.3 ... 46)		
Hadgem3 ensemble		0.84 (0.23 ... 3.2)	1.6 (-14 ... 19)		
CMIP6					
ACCESS-CM2	7.6 mm/day	10 (1.7 ... 80)	17 (3.4 ... 33)	1.9 (1.4 ... 2.7)	5.7 (2.5 ... 9.0)
CanESM5	7.0 mm/day	2.1 (0.72 ... 4.9)	7.9 (-3.0 ... 20)	1.4 (1.1 ... 1.7)	5.5 (0.89 ... 9.1)
GFDL-ESM4	6.2 mm/day	1.3 (0.20 ... 6.7)	2.4 (-13 ... 19)	1.3 (0.83 ... 1.8)	3.2 (-1.8 ... 7.5)
HadGEM3-GC31-LL	7.6 mm/day	3.1 (0.98 ... 10)	9.2 (-0.12 ... 19)	1.4 (1.1 ... 1.8)	4.0 (0.92 ... 6.9)
MIROC6	8.0 mm/day	74 (0.91 ... 8.3e+4)	32 (-0.79 ... 70)	1.6 (0.71 ... 2.8)	4.2 (-2.5 ... 10)

5.3 Results seasonal precipitation

Table 5.3.1: *Similar to Table 5.1.1 but for seasonal precipitation in region South.*

		past - present		present - future	
Model / Observations	**Threshold for return period 20 yr [mm/6months]**	**Probability ratio PR [-]**	**Change in intensity ΔI [%]**	**Probability ratio PR [-]**	**Change in intensity ΔI [%]**

observations	806.204	3.6e+2 (8.8 ... 4.7e+4)	25 (8.8 ... 41)		
HadGEM3					
hadgem3_r1i1p11	6.6e+2	0.50 (0.0049 ... 29)	-4.4 (-26 ... 19)		
hadgem3_r1i1p12	6.8e+2	0.19 (0.023 ... 1.6)	-13 (-28 ... 3.8)		
hadgem3_r1i1p13	7.0e+2	0.73 (0.030 ... 38)	-2.0 (-21 ... 18)		
hadgem3_r1i1p14	6.9e+2	2.0 (0.049 ... 7.3e+2)	3.9 (-16 ... 29)		
hadgem3_r1i1p1	7.2e+2	4.1 (0.052 ... 1.8e+3)	7.7 (-13 ... 34)		
hadgem3_r1i1p3	7.0e+2	2.3 (0.083 ... 3.4e+3)	4.8 (-15 ... 31)		
hadgem3_r1i1p4	7.0e+2	1.2 (0.022 ... 2.0e+2)	1.2 (-21 ... 30)		
hadgem3_r1i1p5	7.0e+2	0.82 (0.053 ... 18)	-1.2 (-17 ... 15)		
Hadgem3 ensemble		0.60 (0.18 ... 2.3)	-1.3 (-8.4 ... 5.9)		
CMIP6					
BCC-CSM2-MR	8.7e+2	2.1e+2 (8.7 ... 2.2e+4)	21 (7.2 ... 37)	2.8 (1.1 ... 6.1)	4.6 (0.37 ... 9.2)
CESM2	7.9e+2	4.1 (0.33 ... 1.3e+2)	6.7 (-5.1 ... 19)	1.6 (0.72 ... 3.2)	2.3 (-1.4 ... 5.5)
HadGEM3-GC31-LL	7.6e+2	4.9 (0.76 ... 22)	7.2 (-0.95 ... 14)	1.4 (0.83 ... 2.1)	1.5 (-0.84 ... 3.8)
MIROC6	7.7e+2	2.0 (0.098 ... 1.8e+2)	3.6 (-11 ... 23)	0.99 (0.33 ... 2.1)	-0.028 (-4.7 ... 4.2)
MRI-ESM2-0	8.1e+2	9.9 (0.77 ... 2.0e+2)	10 (-1.2 ... 22)	1.5 (0.58 ... 3.0)	1.8 (-1.9 ... 5.6)

6 Hazard synthesis

For the event definitions described above we evaluate the influence of anthropogenic climate change on the events by calculating the probability ratio as well as the change in intensity using observations and climate models. Models (and HadGEM3 ensemble members) which do not pass the evaluation described above are excluded from the analysis. The aim is to synthesise results from models that pass the evaluation along with the observations-based products, to give an overarching attribution statement. Figs. 6.1 to 6.5 show the changes in probability and intensity for the observations (blue) and models (red) for the SSI on stormy days for the UKIre and North and South domains, for the precipitation on stormy days for the UKIre domain, and for the Oct-Mar precipitation for the South domain. Before combining them into a synthesised assessment, a term to account for intermodel spread is added (in quadrature) to the natural variability of the models if the spread is larger than expected from natural variability alone. This is shown in the figures as white boxes around the light red bars. The dark red bar shows the model average, consisting of a weighted mean using the (uncorrelated) uncertainties due to natural variability plus the term representing intermodel spread (i.e., the inverse square of the white bars). In the model average, the results of the HadGEM3 model are combined to one single model result first, and this is synthesised together with all CMIP6 model results. Observation-based products and models are combined into a single result in two ways. Firstly, we neglect common model uncertainties beyond the intermodel spread that is depicted by the model average, and compute the weighted average of models (dark red bar) and observations (dark blue bar):

this is indicated by the magenta bar. As, due to common model uncertainties, model uncertainty can be larger than the intermodel spread, secondly, we also show the more conservative estimate of an unweighted, direct average of observations (dark red bar) and models (dark blue bar) contributing 50% each, indicated by the white box around the magenta bar in the synthesis figures.

6.1 SSI on stormy days

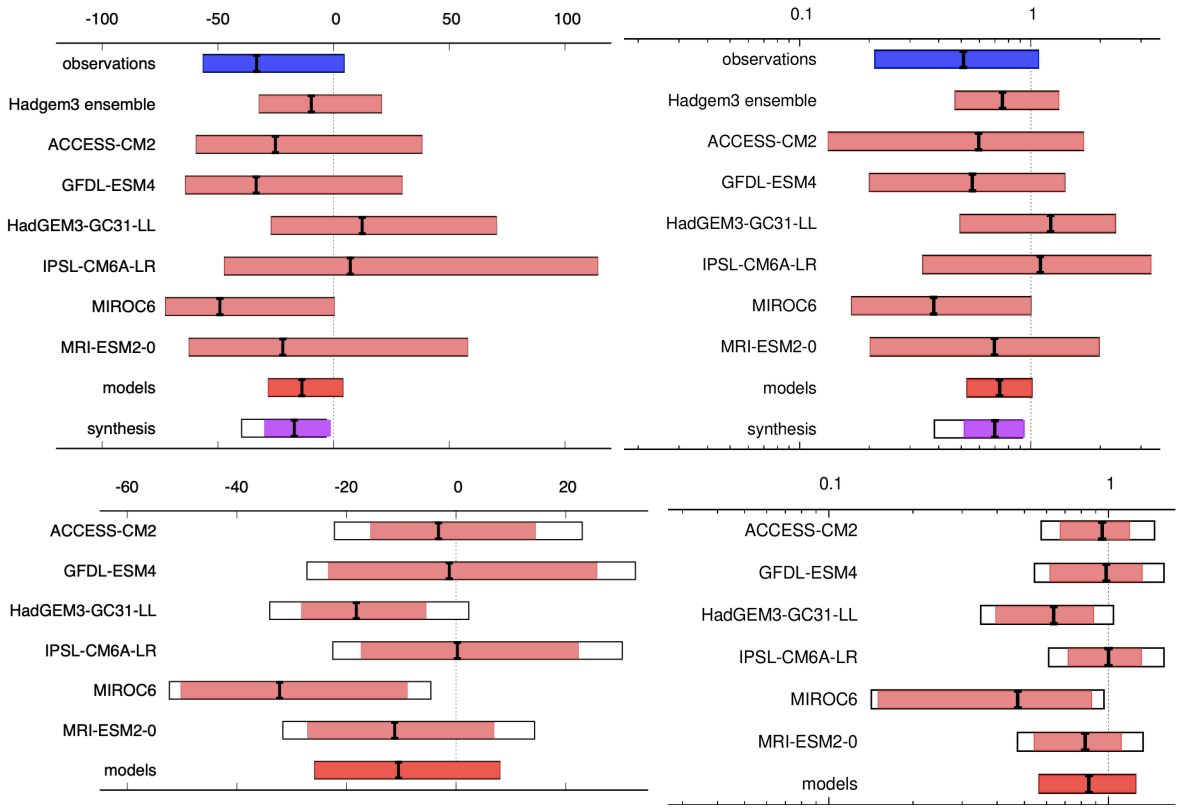

Fig: 6.1: Synthesised changes for mean SSI on stormy days in the UKIre domain. Changes in intensity (left) and PR (right) are shown for a historical period comparing the past 1.2°C cooler climate with the present (top row) and for a future period, based on model projections only, comparing the present and a 2°C warmed climate (bottom row).

Figure 6.1 displays the synthesised intensity change and probability ratio for mean SSI on stormy days for region UKIre. There is relatively good agreement between observations and models so we report the weighted synthesis results – a best estimate of -17.0% with a 95% CI of -29.9.7% to -1.46% in intensity change and, for probability ratio, a best estimate of 0.699 with a 95% CI of 0.516 to 0.936. The changes in PR signify that the probability of occurrence was a factor 1.43 (1.06 to 1.94) greater in the past or, equivalently, the average SSI on stormy days has been reduced by 30% (6% to 48%).

This decreasing trend is continuing with future warming. We find an intensity change of about -10.5% (-25.8% to 7.97%) and a probability ratio of 0.851 (0.566 to 1.25) between the present and a 2°C warmed climate.

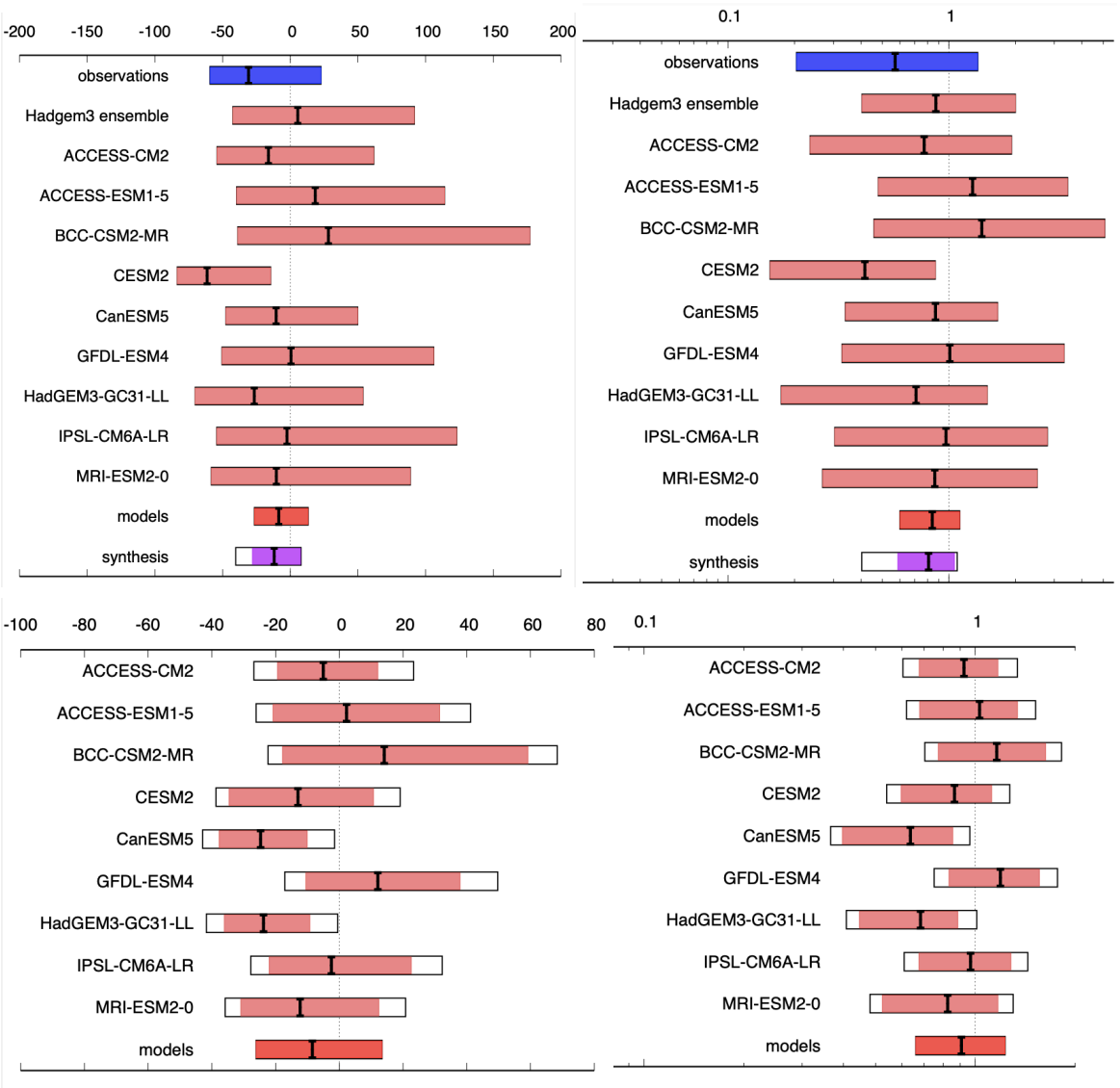

Fig 6.2: Same as for Fig. 6.1 but for the North domain.

Figure 6.2 and 6.3 display synthesised results for mean SSI on stormy days for the North and South domains respectively. As for the UKIre domain, there is relatively good agreement between observations and models, so we report the weighted synthesis results for the historical period showing a decreasing trend in both regions. While the trend is statistically significant when looking at the whole region, this is not the case in each region separately.

For the North domain historical period we find a change of intensity of -11.9% (95% CI: -28.0% to 7.67%) and a probability ratio of 0.809 (95% CI: 0.587 to 1.06).
For the future period we find an intensity change of about -8.46% (95% CI: -26.1% to 13.4%) and a probability ratio of 0.908 (95% CI: 0.661 to 1.23) between the present and a 2°C warmed climate.

For the South domain historical period we find a change of intensity of -32.9% (95% CI: -62.7% to 23.7%) and a probability ratio of 0.679 (95% CI: 0.372 to 1.18).
For the future period we find an intensity change of about -9.19% (95% CI: -43.1% to 45.1%) and a probability ratio of 0.914 (95% CI: 0.495 to 1.68) between the present and a 2°C warmed climate.

Summarising, for all three domains we find a slightly negative historical trend in SSI intensity on Oct-Mar stormy days and in the probability of a 'Oct-Mar SSI on stormy days' similar to or exceeding

that for the 2023/24 season, with best estimates in intensity change ranging from about -39% to -23% and in PR from about 0.7 to 0.8. The latter means that the probability of a similar event was a factor 1.25 to 1.43 times larger in the past, or equivalently, there has been a 20% to 30% decrease in frequency of similar Oct-Mar events. We find that for the models assessed in this analysis this trend may continue into the future. As the results for the North and South domains are relatively similar to the UKIre domain, with similar orders of magnitude best estimates for intensity changes and PRs, we choose to focus on just the UKIre domain for the communication of precipitation results for SSI stormy days (Section 6.2) in our main findings.

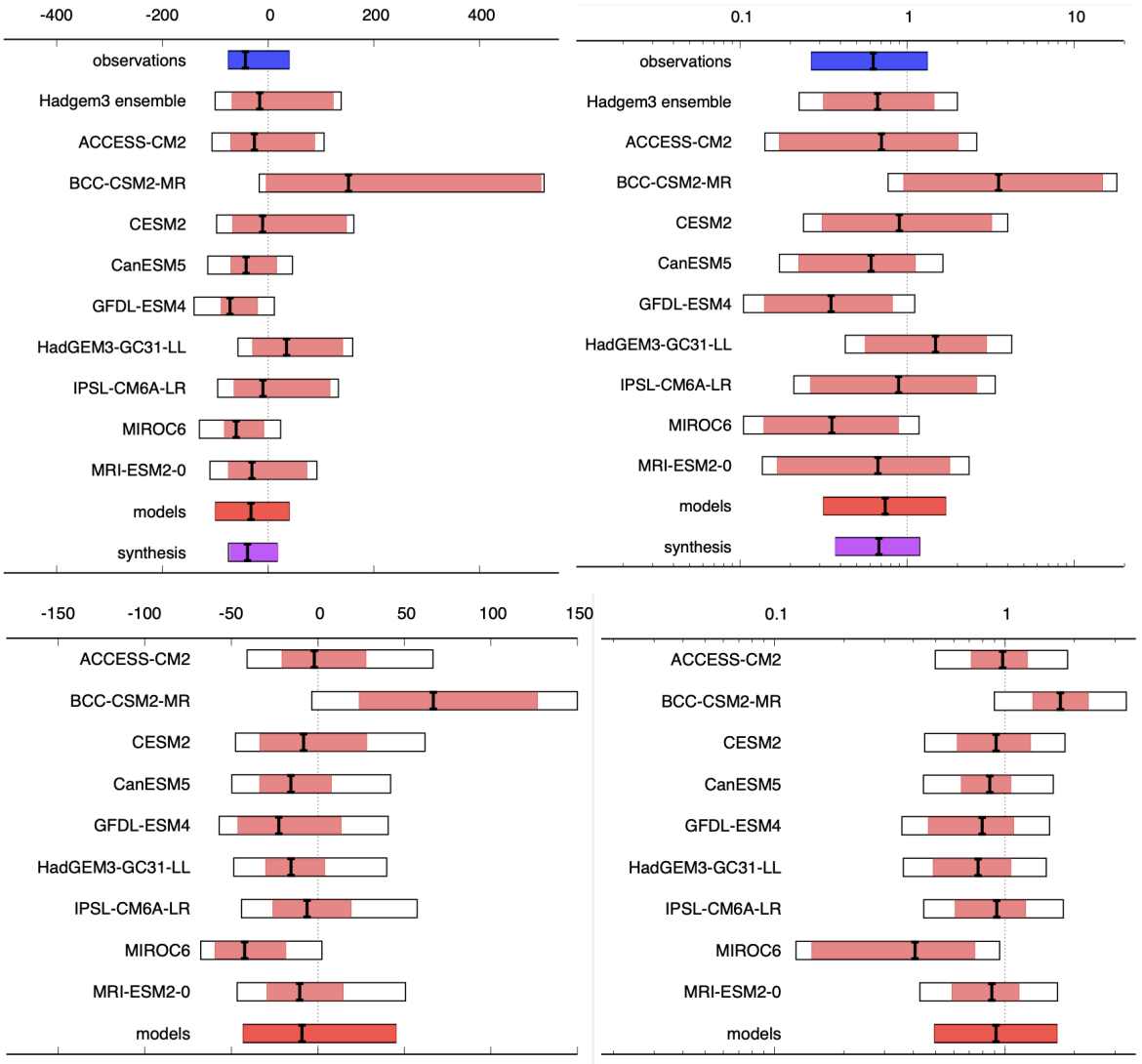

Fig 6.3: Same as for Fig. 6.1 but for the South domain.

6.2 Precipitation on SSI stormy days

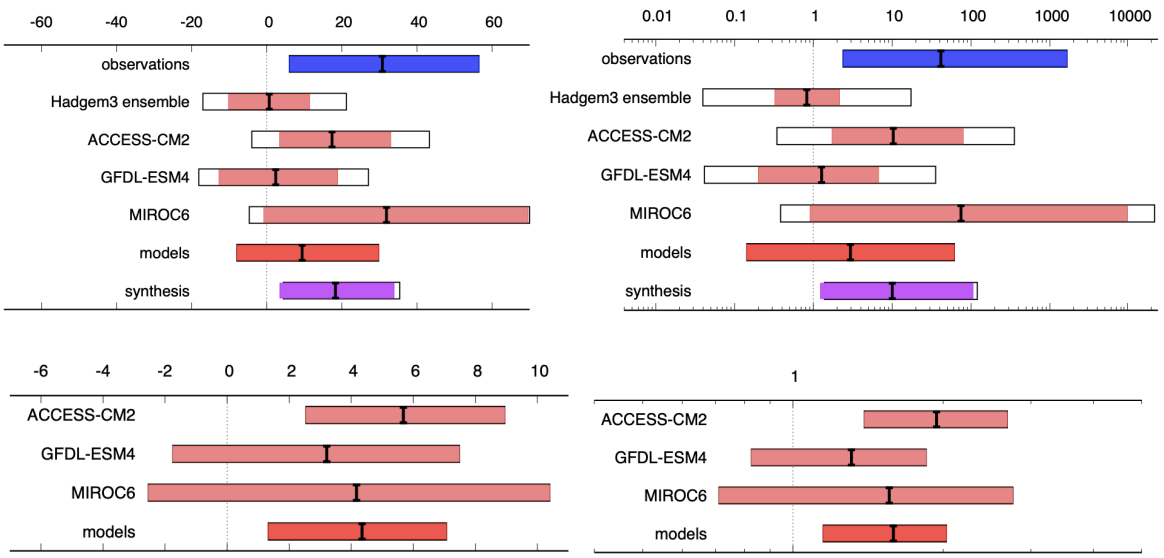

Fig 6.4: Synthesised changes for mean precipitation on stormy days in the UKIre domain. Changes in intensity (left) and PR (right) are shown for a historical period comparing the past 1.2°C cooler climate with the present (top row) and for a future period, based on model projections only, comparing the present and a 2°C warmed climate (bottom row).

Figure 6.4 displays the synthesised changes in mean precipitation on stormy days. Here there is reasonable overlap between the observational and synthesised model uncertainties and the sign of the change is the same – towards more precipitation with climate change. We report the weighted synthesised average (magenta bar), giving a 18.3% (95% CI: 3.49% to 33.9%) increase in intensity and a probability ratio of 10.0 (1.23 to 106), showing that the amount of precipitation occurring on storm days in 2023/24 has become about 10 times more likely.

For the future, using model simulations only, we find an intensity change of about 4.35% (1.33% to 7.07%) and a probability ratio of 1.59 (1.15 to 2.03) between the present and a 2°C warmed climate.

6.3 Oct-Mar seasonal precipitation

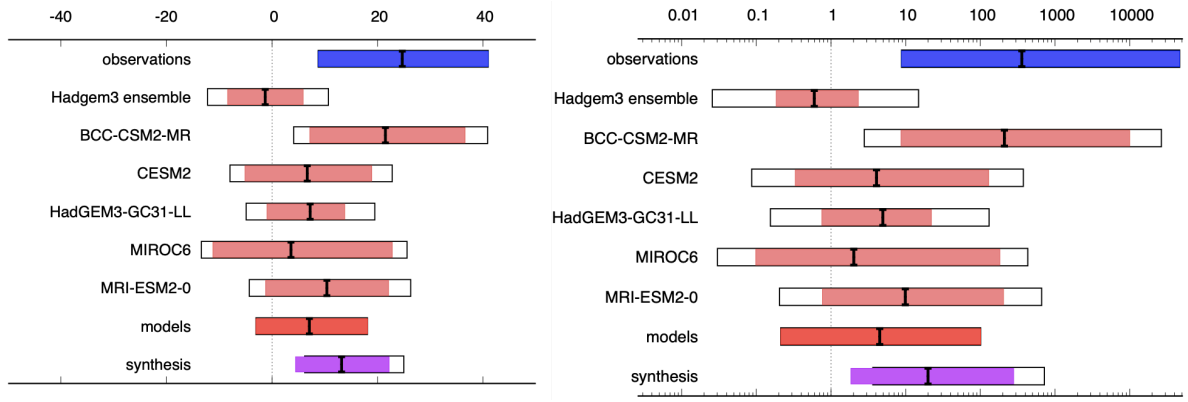

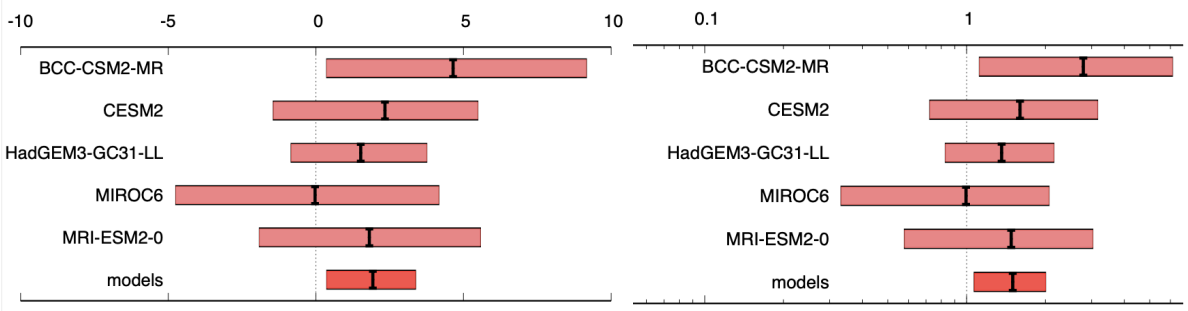

Fig. 6.5: Synthesised changes for Oct-Mar seasonal precipitation totals in the South domain. Changes in intensity (left) and PR (right) are shown for a historical period comparing the past 1.2°C cooler climate with the present (top row) and for a future period, based on model projections only, comparing the present and a 2°C warmed climate (bottom row).

Figure 6.5 displays the synthesis of changes in Oct-Mar total precipitation in the South domain. Although there is some overlap of the observational and synthesised model uncertainties, the models (with the exception of BCC-CSM2-MR) systematically show smaller changes in intensity and frequency than found in observations. We therefore report the unweighted synthesised average (white synthesis bar).

There is a positive change in intensity between the past and the present, with the 95% confidence interval ranging from 6.2% to 25%, using the unweighted average. The unweighted synthesised PR results shows that the chance of Oct-Mar precipitation in excess of the 2023/24 total has increased by a factor of 3.63 to 722 (95% CI) between the past and present.

For the future, model synthesis indicates a further change in intensity between now and a 2°C warmed world of about 1.93% (95% CI: 0.373% - 3.357) and a further factor increase in frequency of 1.5 (95% CI: 1.07-2.0). This estimate is based on model simulations only. In the historical period, the observations are indicating positive changes in intensity and probability that are larger than in the models. Therefore the model-based estimates for the future period may be on the conservative side.

7 Summary and Discussion

Here, we study storminess (both wind and rain) through the lens of the 2023/24 storm season (October to March), with 11 storms named by the Western Europe storm naming group of KNMI, Met Éireann and the Met Office and a further three named by other groups that affected the Western region. As well as some of these storms bringing rainfall that caused flooding, October 2023 to March 2024 was the second wettest Oct-Mar period on record for the UK since records began in 1836, the third wettest for Ireland with records going back to 1941, and the wettest in our 'south' (Figure 2.3.1, including much of Ireland) domain since 1951/52. Therefore, we chose three aspects for study: the storminess in terms of wind using the SSI, the rainfall on stormy days, and the Oct-Mar total rainfall.

For PR and ΔI it is found that, the models align well with observations in SSI on stormy days (that is, days when SSI exceeds its 90th percentile value), but for both of the precipitation-based indices there is a tendency for models to underestimate the changes in precipitation. While there are two different model framings used, the SST-driven model HadGEM3 does not notably deviate in behaviour from the CMIP6 ocean-atmosphere coupled models; however, it is on the lower end of the model spectrum

for the precipitation-based indices with no significant changes in intensity or probability ratio, but with overlapping confidence intervals the general result. Combining lines of evidence from the synthesis results of the past climate, results from future projections and physical knowledge we communicate the best estimate of projected changes in the three aspects of this study.

Our results show a decreasing trend in storminess with increasing GMST, but we note that this may be due to thermodynamic and dynamic effects in combination with the fixed domain. For example, geographical shifts in peak 'storminess' (for example, caused by a systematic shift in the jet stream due to climate change) could also account for a trend over a fixed domain. A possible shift in the jet stream was the motivation for us to explore SSI in the northern and southern halves of our domain (Figure 2.3.1), but these subdomains both show non-significant (negative) trends in SSI, perhaps due to these domains being smaller; it remains unclear if the decreasing trend in storminess is linked to shifts in the storms' average location or the jet stream. The decreasing trend may also be specific to the SSI as a measure of storminess and the time period considered. Previous studies overall show a mixed picture in recent storminess trends over the UK and Ireland, with some studies finding a positive trend, some negative and others no trend, likely due to dependence on the time periods analysed (Feser et al., 2015). Looking to future projections, previous studies have found an increase in windstorm number and intensity over the UK (Feser et al., 2015; Pirret et al., 2023). This includes a weak increase over the UK in the SSI metric is examined in different data sets such as the UK Climate Projections (Bloomfield et al., 2024; Manning et al., 2024) and in CMIP6 data (Little et al., 2023), and when a 'storm tracking' approach is taken with CMIP6 data (Priestley and Catto, 2022). Furthermore, combining the storm hazard with vulnerability and exposure data highlights the uncertainty in potential future damage due to the range of results when examining windstorms in climate models (Severino et al., 2024). However, we have focussed on the period October to March every year to compass the named storms this year, but some studies of winter storms focus on December, January and February, so may indicate different processes or trends at the start and end of the season. While the current study finds tendencies for decrease in the average value of SSI on 'stormy days' (when SSI exceeds its 90th percentile) over the UK for all three study areas, the broad range of outcomes found in other studies indicates that further synthesis work is required, to better understand these differences.

For rainfall on stormy days, we find an increasing trend but of different magnitudes in model and observations. While this could be interpreted as the climate models being more conservative, this could be related to the sampling of the natural variability, year-to-year and on longer timescales. It is possible that the observations show one realisation where the natural variability works with the overall trend due to climate change and reinforces the trend, whereas in the models some have a similar reinforcement but in others the natural variability works against the overall trend, resulting in a multi-model average trend smaller than that observed.

The models also project an increasing trend in rainfall on stormy days into the future. This agrees with the IPCC (AR6) and with other studies examining rainfall, for example that UK heavy winter rainfall events are projected to become heavier but with substantial year-to-year variability (E. Kendon et al., 2023, Figures 9 and 10). We also find our results of a weak trend in storminess combined with an increase in precipitation on stormy days consistent with studies that have identified an increasing risk in the compound hazard of wind and rain in the UK (Bloomfield et al., 2024) and in the UK and Ireland (Manning et al., 2024), with more of the change from increased rainfall than wind (Manning et

al., 2024). Overall, we are confident that the rainfall on stormy days is increasing and will continue to increase in future, but we caveat that the size of that increase is sensitive to the natural variability.

For the seasonal average rainfall, this study shows that the high value seen in 2023/24 was partly attributable to climate change, although as with other rainfall metrics natural variability will also have played a part. Increasing rainfall is consistent with trends in recent observations, for example that UK winters in the period 2013-2022 have been 10% wetter than 1991-2020 and 25% wetter than 1961-1990, with the top five wettest winters all occurring since 1990 (M. Kendon et al, 2023); a slight increasing trend is also observed in autumn rainfall since the pre-industrial era (M. Kendon et al, 2023, Figure 33). Ireland's winter rainfall increased by 7% in the period 1991-2020 with respect to the 1961-1990 period, and autumn rainfall by 5% when comparing the same periods (Coonan et al., 2024). UK winter rainfall is also projected to increase in the future (UKCP, 2022), but the projected trend in autumn rainfall is less clear (E. Kendon et al., 2023, Figure 5). For Ireland, in a +1.5C global warming scenario, both annual and winter precipitation is projected to increase. Again, the increasing trend is statistically robust but caveat that the magnitude may be affected by the natural variability.

For the first time, we identify that the rainfall on stormy days (as quantified by SSI) has increased due to climate change, and is projected to increase into the future. On the one hand, we consider our results for both rainfall metrics robust, given that they align well with previous studies and with current understanding of how the physical processes driving rainfall will evolve in our changing climate. On the other hand, our results around storminess (i.e. how high the SSI becomes on days with SSI over the seasonal 90th percentile) show a decreasing trend, but this is less well-understood particularly in the context of existing literature and would benefit from further investigation.

8 Vulnerability and exposure

Affecting large geographies spanning both rural and urban contexts, the storms led to significant and compounding impacts across sectors. It is important to examine how vulnerability and exposure (V&E) influenced the storm consequences to gain a greater understanding of drivers of impacts, which, coupled with hazard attribution results, can inform future preparedness and adaptation interventions. Elements that affected V&E to winter storms during the 2023/24 period were identified via a workshop with British Red Cross (BRC) staff and volunteers who were actively involved in emergency response to these events (referenced as 'BRC observations'), and a review of literature including news articles, gray literature and academic publications. Identified V&E factors included (i) housing, (ii) financial, and (iii) health and well-being characteristics of individuals.

8.1 Intersecting vulnerabilities

The severity of climate impacts is influenced by the vulnerability and exposure (V&E) to hazards (Cardona et al., 2012). For example, flooding can have more adverse consequences if properties are in floodplains and if the population are elderly, less mobile and have limited access to emergency services. V&E varies across areas as a result of economic, social, geographic, demographic, cultural, political, institutional, infrastructural and environmental factors (Cardona et al., 2012, Thomas et al., 2018, OECD, 2018). People may be vulnerable during emergencies for several reasons including

health, economic, social, discrimination or through situational and geographic factors (BRC, 2024). These vulnerabilities can interact and intersect, compounding their effect.

8.1.1 Housing

Housing quality, location and situation all influenced exposure and vulnerability to these named storms. Heavy rainfall and excess moisture can lead to damp, mould growth, and costly repairs (Kovats and Brisley, 2021). Buildings at risk from river flooding include those in floodplains (areas of land adjacent to rivers which experience flooding during periods of high discharge FloodHub, 2018), and areas with low levels of green and blue infrastructure, which have high levels of impermeable surfaces (NIC, 2022). One in 13 new homes built in England in the past decade has been built in floodplains (Aviva, 2024). There are also challenges with lack of awareness of those at risk. Research by the BRC (2022) found that awareness of flood risk is lower amongst those living in high risk areas and those with heightened vulnerability to floods. Limited risk perception/awareness and the cost-of-living crisis limit uptake of and access to Property Flood Resilience (PFR) measures such as flood doors and automatic air bricks, decreasing resilience (Glencross et al, 2021; BRC, 2022).

People living in mobile homes on coastal caravan sites have heightened vulnerability, as indicated by increasing emergency response callouts and news reports of holiday home evacuations (BBC, 2023). Around 28% of caravan and camping sites in England and Wales are at flood risk, with over two-thirds at either significant or moderate flood risk (Defra, 2012). Residents of basement flats are also at greater risk with nearly half of London's 33,205 basement properties in commercial use exposed to surface water flooding (Zurich Insurance, 2022). Maintenance of houses and surrounding areas also influences risk. For example, there is currently an investigation into the gully clearing programme of Nottinghamshire Country Council where over 900 properties were flooded as a result of Storm Babet (BBC, 2023). Lastly, people experiencing homelessness are adversely affected by extreme weather as they lack shelter and security. Many local authorities activated their Severe Weather Emergency Protocol (SWEP) to support homeless people during the winter storms (Mayor of London, 2023). Residents may also become homeless due to storm damage. In Portadown, Northern Ireland a dozen residents chose not to move away from their damaged properties as they feared being declared homeless by the state and placed anywhere in the country, posing an inconvenience to maintain employment and education in the same place (BBC, 2023; BRC observations). Altogether, flooding aggravates the risk of displacement and homelessness, and can intensify competition in housing markets which are already challenged by the highest rental prices in the UK in 14 years (Geraghty, 2024; Steed, 2024).

8.1.2 Economic or financial vulnerability

Living in poverty or on low incomes affects how well people can prepare for, respond to and recover from extreme weather events, including storms. People experiencing social deprivation in the UK tend to live in areas with greater exposure to flooding (from all sources) (EA, 2022). Income affects access to flood insurance, with lower income households and those in rented or social housing less likely to have insurance (Sawyers, 2020).

Polling by the BRC (2022) suggests that financial barriers to insurance are widespread, with 15% of UK adults without buildings or contents insurance, primarily due to affordability. Limited access and uptake of insurance influences financial vulnerability and removes safety nets. The storms and

associated flooding caused weather-related home insurance claims in the UK to rise by more than a third, reaching a record £573m according to the Association of British Insurers (ABI, 2024) as a result of successive storms including Babet, Ciaran and Debi causing flooding and burst pipes (Guardian, 2024). Those without insurance/financial means struggle to rebuild or repair after severe weather – for example anecdotal evidence from emergency responders suggests that some people were unable to run dehumidifiers provided to address risk of damp and mould in flooded properties following the storms.

Prolonged wet weather also impacted the agricultural sector with losses of crops, livestock, and livelihoods, leading to concerns over potato shortages and reductions to beef farmers' herds (Irish Independent, 2024a; RTE, 2024; Irish Independent, 2024b). Environmental regulations were relaxed to aid farmers (Irish Independent, 2024c), but financial repercussions on farms were significant, particularly for milk production (Irish Independent, 2024d; Irish Independent, 2024e). In mid-April, Northern Ireland potato farmers were up to six weeks behind schedule and warned of potential price increases (BBC, 2024).

8.1.3 Health and wellbeing

Those experiencing poor physical or mental health can be disproportionately affected by weather and climate impacts. From a physical health perspective, elderly people, suffering from limited mobility, and in some cases also limited social networks, were often supported more by voluntary and community sector organisations like the Red Cross during and after the storms (BRC observations). BRC observations further suggest that those in transient situations, particularly asylum seekers residing in asylum accommodation, were more vulnerable to the storms given limited autonomy and housing is often left out of local emergency response plans. Flooding also poses health risks due to poor sanitation and spread of infectious diseases which can delay access to the medical attention or medicines they need.

Storms can lead to extensive mental health impacts due to trauma distress when homes and assets are damaged. Flood depths between 30-100cm can result in mental health costs of £3,028 per adult per flood event, and £4,136 by flood water above 1m (EA, 2021). Weather warnings bring back painful memories of previous incidents, resulting in mental stress and anxiety (BRC 2010). Repeated flooding, as seen in Cumbria, England, has been linked to higher levels of depression (French et al., 2019). Displacement, financial strain, and prolonged uncertainty regarding recovery efforts can also erode social cohesion and exacerbate mental health challenges (Greene et al., 2015). The repeated storms during the 2023/24 likely had psychological consequences for those affected. Angus Council, in Scotland, is engaging with residents in Brechin to understand the effects on mental health and wellbeing following storm Babet (Angus Council, 2024).

8.2 Land use land cover changes

Northern parts of the UK and Ireland have experienced the most significant increase in flood events and storm surges across Europe (Blöschl et al., 2019) and the four storms which triggered this study heavily impacted almost all UK regions. Changes in land-use can also exacerbate flood risk (Figure 1).

Figure 1: Schematic of Land-Use Change on Floods

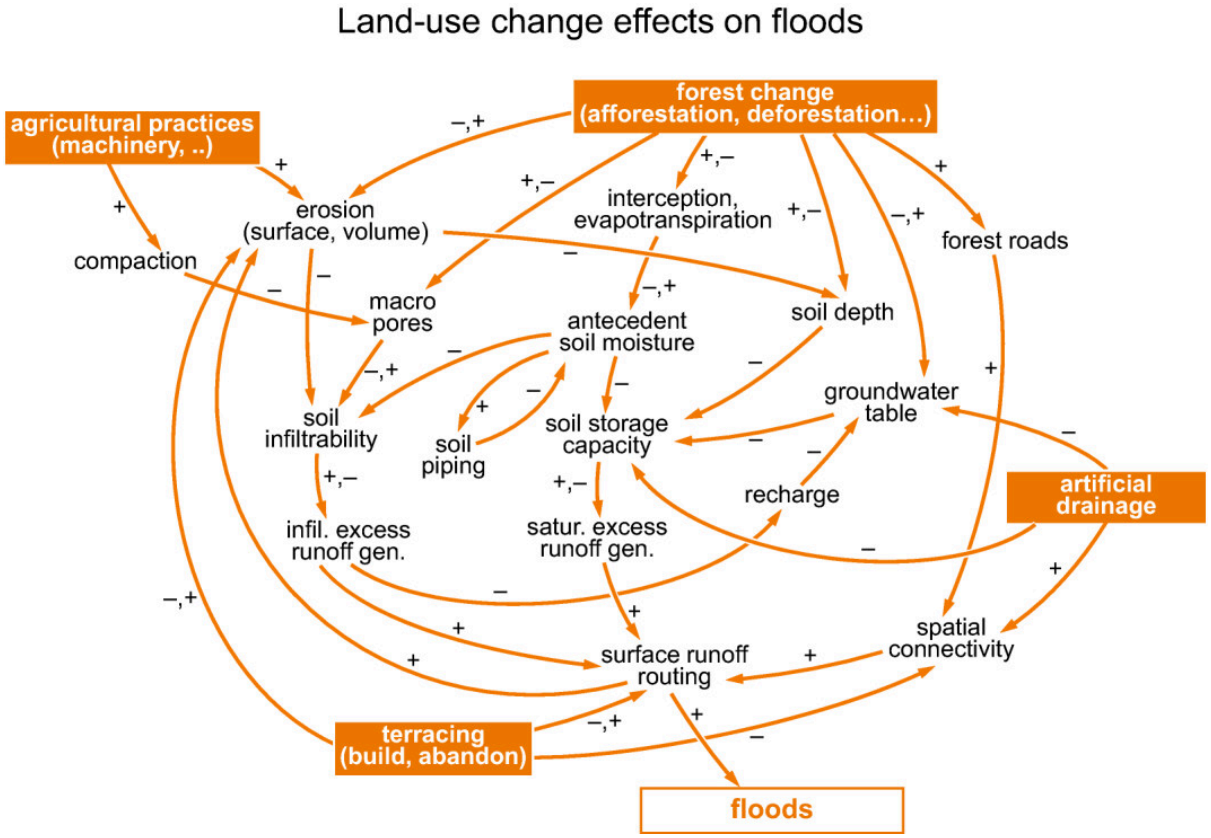

Source: Rogger et al., 2017

The growth of urban regions can raise flood risk as urbanisation replaces natural, porous soil with impermeable materials, such as concrete and asphalt, that diminish infiltration and bypass the ground's natural storage capacities (Wheater and Evans, 2009; LGA, n.d.). These materials increase overland flow and reduce the time to peak flow during rainfall, elevating flood risk and severity (ibid). Similar effects occur through deforestation and grassland erasure, reducing the ground's natural storage capacity (Rogger et al., 2017; Cooper et al., 2021).

In urban areas, surface runoff is gathered through piped storm-water drainage systems and rapidly transported to the nearest stream. However, the storm surges from these storms overwhelmed local drainage systems, and they lacked adequate procedures to reduce surface water flooding (Clarke, 2023; EA, 2023; Fisher, 2024). Moreover, there has been an increase in people paving or building over their vegetated gardens, referred to as 'urban creep' (Rowland et al., 2019). Soil type and quality can determine flood risk across the UK and Ireland (Boorman et al., 1995).

Agricultural intensification across the UK also increases flood risk. Approximately 70% of the UK's landscape is agricultural (UK Government, 2023), of which, a significant portion of this country's most productive agricultural land is located on floodplains or along the coastline, increasing flood risk and vulnerability (CRPE, 2022). Agricultural practices can cause deforestation of woodland habitats, and soil compaction due to heavy machinery and livestock that reduce natural soil infiltration and ground storage capacity (Rogger et al., 2017; Cooper et al., 2021). This increases flood risk. The type of crop planted can impact flood risk, for instance, cover crops, including radish and buckwheat, can help to stabilise the soil and reduce surface runoff (Cannon et al., 2023). The consequences of such

land-use change, if not managed appropriately, can increase crop loss to waterlogging, which is expected to rise in the UK (Kaur et al., 2019), and additionally increase the flood risk of nearby settlements. There is growing political and public interest in how managing the UK's broader rural landscape can enhance the country's flood defence system, particularly through natural flood management (NFM) that implements natural processes to reduce flood risk (UK Government, 2024). Regenerative farming values aim to enable the nutrients, soil, water, land, and other natural assets to renew themselves, as opposed to conventional farming practices that exhaust the capacities of these natural resources by working *against* the land (natural hydrological and ecological processes) (Rodale, 1983). This approach also has the potential to mitigate climate change through its increased carbon sequestration outcomes (Kastner, 2016), helping to mitigate flood risk further for agricultural land and nearby settlements.

Flooding factors in urban areas are complex, involving interactions among assets owned by different entities, such as public sewers, private drains, highway drainage, and riparian watercourses (Jenkins, 2020). Similar complexities arise in rural areas, where land drainage and agricultural surface water runoff can overwhelm or contribute to the obstruction of highway and other drainage systems in towns and villages (ibid).

8.3 Urban planning

The UK's flood defence strategy incorporates extensive hard-engineered measures in and around major urban areas and flood banks, and smaller-scale engineering measures for rural areas, agricultural land and coastal protection structures. While traditional urban planning techniques, which often apply less porous materials such as tarmac and concrete over water-absorbent topsoil, can exacerbate flood risk, the introduction of contemporary NFM, blue-green urban infrastructure and nature-based solutions help to reduce flood risk in cities and towns across the UK (O'Donnell et al., 2017), and provide a host additional biodiversity, and health and wellbeing benefits (Brown and Mijic, 2019).

Through traditional urban planning techniques, many natural waterways are presently constrained within narrow channels, frequently lacking adequate maintenance (LGA, n.d.). This practice of culverting watercourses in urban zones was widespread and intended to increase land availability for development (ibid). However, culverting substantially heightens the risk of flooding due to constricted flow within piped sections, susceptible to blockages, and an increase in water transportation to nearby streams and rivers, therefore increasing flood risk and vulnerability, especially during storm surges (Wheater and Evans, 2009; LGA, n.d.). New urban developments also have the potential to substantially impact flood risk through increasing surface water flooding unless measures are taken to implement data-driven tools, such as CityPlan-Water, that drive sustainable urban development through, for example, adequately designing water-neutrality into housing (Puchol-Salort et al., 2022). Vulnerability is intensified as large portions of the UK's drainage infrastructure is ageing and requires substantial maintenance or replacement (Jenkins, 2020). Development historically occurred in regions with a comparatively high susceptibility to flooding, often with buildings constructed closely along riverbanks, river basins and coastlines. These circumstances increase the vulnerability of urban areas to river and coastal flooding in the present day, including some of the areas most affected by the four storms this study refers to. For example, Storm Ciaran greatly affected the UK's coastal cities across the South Coast, such as Dover, Devon and Dorset (UK Met Office, 2023a). Furthermore, as well as

affecting urban settlements along the UK's East Coast, Storm Babet also affected many urban settlements within close proximity to riverbanks across Yorkshire and the Humber region (UK Met Office, 2023b).

Major cities including Manchester (Manchester City Council, 2022), Belfast (Belfast City Council, 2020), Cardiff (Edmond and Geldard, 2023), and Newcastle (O'Donnell et al., 2017), have started to adopt NFM, blue-green infrastructure and nature-based solutions (NbS) into their urban design to improve flood risk in addition to biodiversity levels, climate change mitigation and adaptation, and human health and wellbeing (Smith and Chausson, 2021; Brown and Mijic, 2019). Such initiatives combine natural features, including wetlands, green roofs and walls, ponds, rainwater gardens and restoring river channels, in the urban environment to enhance urban water capture and storage systems (Scottish Water, 2024; Brown and Mijic, 2019). These programmes also aid with the creation of climate resilient cities and towns that incorporate adaptive measures to protect and promote urban hydrological and ecological values. Water companies and local flood authorities utilising such practices include, the Welsh Water RainScape programme (Welsh Water, 2016), Northumbrian Water's Rainwise surface water initiative (Northumbrian Water, 2016), and Thames Water's sustainable drainage schemes (SuDS) and NbS (Thames Water, 2023). Similarly, Dublin (Dublin City Council, 2021; Dublin City Council, 2022), Cork (Cork City Council, 2022), and Galway (Galway City Council, 2021; Galway City Council, 2022) aims to restore biodiversity and ecosystems through NbS including initiatives such as river restoration, developing a wildfire corridor, constructing wetlands, and promoting green roofs and walls, SuDS, and increased urban tree cover. In Ireland, flood relief projects have been integrating nature-based solutions alongside traditional engineering solutions for over 20 years.

8.4 Disaster risk management

Flood risk in the UK and Ireland is driven by challenges such as more frequent extreme weather events, sea level rise, population growth, and urbanization, including the expansion of residential areas into flood-prone zones (Puchol-Salort et al., 2022; McGlone, 2023). This necessitates a multifaceted approach to adaptation and flood protection based not only on the climate of today but of the future, which is especially crucial considering the attribution findings of climate change-induced rainfall associated with storms in the region. It is also important to acknowledge the so-called adaptation effect in this context. When a perceived increase in protection due to improved flood management infrastructure allows new developments to be built in their vicinity, the onset of stronger events can cause more damage (Mijic et al., 2023).

8.4.1 Adaptation and flood risk management policy

Policy plays a crucial role in mitigating the adverse impacts of flooding on communities and infrastructure. Climate change adaptation policy in the UK is directed primarily from the Climate Change Act of 2008, which established the Climate Change Committee (CCC) to complete a five-yearly Climate Change Risk Assessment (CCRA) (UK Climate Risk, n.d.), followed by a National Adaptation Programme (NAP), which combine to form the foundations of adaptation policy in the UK. The Climate Change Act of 2008 provides the policy framework for both mitigating and adapting to climate change and its risks. The Flood and Water Management Act 2010 serves as an additional cornerstone of flood risk management, delineating the roles and responsibilities of various

authorities such as the EA and local flood authorities (EA, 2020; LGA, n.d.). Additionally, the National Flood and Coastal Erosion Risk Management Strategy for England emphasizes resilience-building and climate adaptation through diverse measures, including soft engineering approaches (EA, 2020). Furthermore, the National Planning Policy Framework mandates a risk-based approach to development location and promotes sustainable drainage systems (LGA, n.d.). The EU Floods Directive, incorporated into UK law, mandates the production of flood risk assessments, hazard maps, and management plans (LGA, n.d.). Between 2021-2027, the government has committed to investing £5.2 billion in flood risk management projects (UK Parliament, 2024).

While the UK government coordinates adaptation policy in England, and provides the foundation for policy throughout the UK, much of UK policy output focuses on England and non-devolved matters. The devolved nations therefore have additional policy framework to respond more specifically to climate adaptation and flood risk management. Policy and progress differs across the devolved administrations of the UK. For example, the Climate Change (Scotland) Act 2009 (Government of the UK, 2009) established Scotland's statutory framework on climate change adaptation, requiring a Scottish Climate Change Adaptation Programme (SCCAP) (Scottish Government, 2019) to address the Scottish risks identified in the CCRA. The Public Bodies Climate Change Duties (Government of the UK, 2020) established through the Climate Change (Scotland) Act requires relevant public bodies to prepare annual mandatory reports outlining the actions they are taking to address their climate change responsibilities. This information is used to inform the Scottish ministers on their annual progress reports. Northern Ireland has just introduced similar public bodies reporting duties. In Wales, the Wellbeing of Future Generations (Wales) Act 2015 sets out wellbeing goals for Wales including a more resilient Wales, that requires public service boards to consider the most recent CCRA and climate risks to Wales when making wellbeing assessments and suggestions (Future Generations Commissioner for Wales, 2015). The Welsh Environment Act 2016 provides further provisions regarding climate change adaptation (Government of the UK, 2016), and Prosperity for all: A Climate Conscious Wales 2019, sets out how Wales is adapting to the areas of highest risks to climate change impacts (Welsh Government, 2019). Ireland's first statutory National Adaptation Framework (NAF) was published in 2018 (Irish Govt, 2023).

In Ireland, the 2004 National Flood Policy Review identified flood risk prevention as a key priority, leading to the Office of Public Works (OPW) taking the lead in coordinating national flood risk management efforts (OPWs, 2018). The Catchment Flood Risk Assessment and Management Programme provided vital evidence for prioritizing government investment in flood risk management, amounting to €1 billion over the next decade (OPW, 2018). Individual Flood Risk Management Plans for each river basin outline proposed measures, including new flood relief schemes to safeguard properties (OPW, n.d.). Planning Guidelines on Flood Risk Management guide sustainable development practices, while the Minor Works Scheme and Arterial Drainage Maintenance address localized flood issues (Government of Ireland, 2019). The Government Decision of 5th January 2016 agreed to the establishment of a National Flood Forecasting and Warning Service (NFFWS), under the oversight of the OPW. The first stage of the services comprises a Flood Forecasting Centre (FFC), which is operational within Met Éireann since January 2024. The FFC provides flood forecasting from river and coastal sources and related advisory services specifically to Local Authorities and emergency management stakeholders. Stage two plans for the NFFWS, including plans for a public warning service, are under development by the NFFWS Steering Group led by the OPW.

The Irish EPA funded a research project, the Transboundary Adaptation Learning Exchange (TALX), to identify the barriers and enablers of climate adaptation and assess national policy against these across England, Scotland, Wales, Northern Ireland and the Republic of Ireland (TalX, 2024). Within the TalX policy assessment framework elements relating to governance including 'leadership & co-ordination of roles and responsibilities' were explored in each region, highlighting limitations. It was identified that there was more work needed to understand vulnerability and exposure by mapping climate impacts with existing regional data such as health and inequity information to see where the highest vulnerabilities lie (EPA, 2022).

8.4.2 Flood protection

In the UK, significant investments have been made by the government and environmental agencies to bolster flood protection infrastructure. The EA's deployment of flood barriers, non-return valves, and pumps aims to contain water within river channels and safeguard properties during flood events, while restoring peatlands to slow the water flow and creating flood storage areas (EA, 2021; Mittal, 2024). Moreover, planning guidance updates have been implemented to improve to account for flood risk (National Infrastructure Commission, 2023), and substantial funding, amounting to over £6 billion since 2010, has been allocated to protect hundreds of thousands of properties from flooding and coastal erosion (Wallace, 2024). In Wales, the government has allocated over £75 million to managing flood and coastal erosion risk, marking the largest yearly investment in the country's history (Natural Resources Wales, 2024). Notable successes in the UK include the enhanced protection provided during storms such as Babet, Ciaran, and Emma. It is estimated that about 100,000, 13,000, and 75,000 properties were better protected against the respective storms (Wallace, 2024). However, challenges persist, including the overburdened and aging flood defense infrastructure and pressure to balance new development with flood risk (McGlone, 2023). Importantly, concerns have also been raised about how effectively targeted the £6 billion investments have been towards addressing the underlying social vulnerability (England & Knox, 2015). Adequate funding and proactive planning centered on the root causes of flood risk are critical to address these challenges effectively.

In Ireland, statutory planning guidelines and flood relief schemes spearheaded by the Department of Housing, Planning, and Local Government and the OPW have made significant strides in protecting properties from flooding (OPW, 2018). Further, the Forestry Service provides essential guidelines on sustainable forest management, aiding in flood risk management (OPW, 2018). The OPW has spearheaded major relief schemes, shielding over 9,500 properties, with more underway to safeguard an additional 12,000 properties. Additionally, through local authorities, over 500 minor relief schemes have fortified an extra 6,500 properties (OPW, n.d.; OPW, 2018). The OPW's maintenance of river channels and embankments, covering 11,500 and 800 km, respectively, is integral to flood risk mitigation (OPW, n.d.). Moreover, significant governmental investment, totaling €1 billion, underscores a proactive commitment to implementing comprehensive flood risk management strategies, as delineated in the Catchment Flood Risk Assessment and Management (CFRAM) plans (OPW, 2018). Yet, the region faces similar challenges to the UK of rising sea levels and extreme weather events (Environmental Protection Agency, n.d.), necessitating sustained investment and the continuous exploration of natural flood management approaches.

Enhancing flood protection measures in the UK and Ireland requires a holistic approach

encompassing climate-resilient infrastructure development, policy interventions, and nature-based solutions that are well targeted for those facing greatest flood risk. Collaborative efforts between government entities, local authorities, and communities are crucial to building resilience against the escalating threat of flooding in both regions.

8.4.3 Early warning systems

The winter storms of 2023/24 in the UK and Ireland were characterised by forecasting accuracy, albeit with challenges in pinpointing exact timing and intensity. Forecasts warned of an exceptionally stormy winter, indicating a heightened risk scenario (UK Met Office, 2024). Long-range predictions foresaw a colder, drier season, yet emphasised the inherent uncertainties in such forecasts, underlining that long-range forecasting is not an exact science (Real Weather, 2023).

In the UK, the EA operates the flood warning and management (EA, 2020). Utilising an extensive monitoring network and collaborating closely with the Met Office and the Flood Forecasting Centre (FFC), the agency issues flood guidance statements and forecasts tailored to specific locations through various communication channels such as social media, community volunteer networks, and mobile phone alerts (EA, 2020; Government of UK, n.d.). However, issues such as reliance on mobile connectivity persist (Budimir et al., 2022), highlighting the need for improved dissemination methods and infrastructure resilience. Further, anecdotal evidence from people impacted by floods suggests an inadequacy of early action (BRC observations). However, advancements like the expansion of monitoring technologies to remote areas demonstrate ongoing efforts to address these challenges (EA, 2023). Looking ahead, in late 2025, the UK government is set to launch a "next-generation flood warning service", aiming to rapidly communicate impact-based risks to mobile phones (EA, 2023).

In Ireland, flood risk management falls under the jurisdiction of the Department of Public Expenditure and Reform, with responsibility for the Office for Public Works and flood relief. While weather forecasting services are provided by Met Éireann, the Irish Meteorological Service, challenges remain due to the unpredictable nature of storms, compounded by the region's smaller size and shorter water courses (OPWs, 2018; BRC observations). The Government Decision of 5th January 2016 agreed to the establishment of a National Flood Forecasting and Warning Service (NFFWS), under the oversight of the OPW. The first stage of the services comprises a Flood Forecasting Centre (FFC), which is operational within Met Éireann since January 2024. The FFC provides flood forecasting from river and coastal sources and related advisory services specifically to Local Authorities and emergency management stakeholders. Stage two plans for the NFFWS, including plans for a public warning service, are under development by the NFFWS Steering Group led by the OPW.

Robust early warning systems and anticipatory measures are crucial to mitigating the impact of storms and floods. While progress has been made, ongoing collaboration, technological innovation, and community engagement are essential to help translate warnings into action and enhance resilience. Across the UK and Ireland, lack of preparedness exercise and activities also shaped vulnerability. Limited in person training and exercises (knock on from covid detracting priorities and switching to online world) meant that communities were not prepared and were not supported, and evacuations taken into their own hands (BRC observations).

8.4.4 Response and recovery

In response to the floods during the 2023/24 winter storm season in the UK, the government swiftly activated the Flood Recovery Framework to aid those affected. Flooded households can now access immediate relief through cash grants of up to £500, offering crucial support for their basic needs (Department for Levelling Up, Housing and Communities et al., 2023). Moreover, households and businesses severely impacted by the floods will benefit from a significant measure of relief, with 100% council tax and business rates relief provided for a minimum of three months (Ibid.). Shortages of animal feed in Ireland also prompted the establishment of a fodder hotline by the government's agricultural advisory agency (Irish Independent, 2024), while government support packages aimed to mitigate financial losses in cereal production (Irish Independent, 2024b).

Small and medium-sized enterprises (SMEs) in the affected regions are also being supported in their recovery efforts. The Business Recovery Grant, offering up to £2,500, aims to assist these businesses in resuming normal operations, providing a lifeline during this challenging period (Department for Levelling Up, Housing and Communities et al., 2023). Additionally, the government is proactively investing in long-term resilience through the Property Flood Resilience Repair Grant Scheme (Ibid.). Eligible property owners can access grants of up to £5,000 to fortify their homes and businesses against future flooding, underscoring a commitment to not only respond to immediate crises but also to mitigate future risks (Ibid.).

8.5 V&E conclusions

Policy and governance contexts differ across the UK and Ireland. Widespread damages resulted from the 2023/24 winter storms, potentially highlighting the limited implementation of interventions to address climate risks as indicated by assessments of adaptation progress across Scotland (CCC, 2023), England (CCC, 2023), Northern Ireland (CCC, 2023) and Ireland (CCAC, 2023). Effective adaptation requires a thorough understanding of the concepts of exposure and vulnerability, and their dynamics over time. This analysis summarizes evidence that together highlights the need for greater prioritisation of adaptation as a central government policy agenda (across UK and Ireland), and additional resources allocated to address factors influencing vulnerability and exposure to climate risks, including storms and associated flooding.

Data availability

Almost all data are available via the Climate Explorer.